"Novel Joining Technique for Oxide-Dispersion Strengthened Iron Aluminide Alloys"

Contract No. DE-FG03-00ER83041

FINAL REPORT

Reporting Period: 06/04/01 – 12/03/2006
P.I.: Dr. Eugene Dyadko

Prepared By:

Materials and Electrochemical Research (MER) Corporation
7960 South Kolb Road
Tucson, AZ 85706
(520 574-1980

MER #90452

ABSTRACT

Oxide dispersion strengthened ferritic steels are irreplaceable in modern technology due to their unique resistance against creep. In order to enable the wider use ODS materials, it is necessary to develop reliable methods of joining them. The conventional welding methods (arc, plasma, laser, or electron beam) inevitably lead to fluid formation, which, in turn, results in coarsening of the fine oxide particles and thus loss of their ability to confer creep resistance. Direct diffusion bonding has not been successful due to a tenacious alumina scale which forms on the alloy surfaces. Also, usage of interlayers did not result in strong joints, since no interlayers possess the unique properties of ODS ferritic steel.

Plasma-assisted joining is one of the methods that can solve this problem. During bonding, plasma discharges break the oxide scale and intensify the mass transfer. This allows bonding at lower temperatures, thus avoiding disturbance of the microstructure. In order to provide strong butt joints in ODS ferritic steel, unrecrystallized pieces should be bonded. Plasma-assisted butt joining, followed by a recrystallization heat treatment, results in full secondary recrystallization with grain growth across the bonding line. This provides UTS values at 1000^{o}C usually ranging from 70 MPa / 10.1 ksi to 77 MPa / 11.1 ksi. This constitutes from 78 to 86% of the UTS achievable by solid MA-956 at 1000^{o}C. The best result was 88 MPa / 12.8 ksi, which amounts to 98% of the solid MA-956 UTS at 1000^{o}C.

Tube bonding of commercially available recrystallized ODS ferritic steel with plasma-assisted sealing resulted in failure at 49 MPa / 7.1 ksi in 377 hours during step-loading testing at 1000^{o}C. This joint strength falls within the usual range for the strength of solid ODS ferritic steel tubes.

TABLE OF CONTENTS

TABLE OF FIGURES

TABLE OF TABLES

TABLE OF ACRONYMS

A	Ampere
ASTM	American Society for Testing and Materials
C	Celsius
DC	Direct Current
F	Fahrenheit
EDS	Energy Dispersive Spectroscopy
FIB	Focused Ion Beam
h	Hour
ID	Identification
in	Inch
IGBT	Isolated Gate Bi-Polar Transistor
ksi	1000 Pounds Per Square Inch
KW	Kilowatt
KV	Kilovolt
µm	Micron
MER	Materials & Electrochemical Research
max	Maximum
min	Minute
mm	Millimeter
MPa	Mega Pascal
OD	Outside Diameter
ODS	Oxide Dispersion Strengthened
ORNL	Oak Ridge National Lab
SBIR	Small Business Innovation Research
SEM	Scanning Electron Microscopy
TLP	Transient Liquid Phase
TEM	Transmission Electron Microscopy
TTL	Transistor-Transistor Logic
UTS	Ultimate Tensile Strength
V	Volt
WE	Welding Factors
WMT&R	Westmoreland Mechanical Testing & Research

1. Introduction

Improved performance in jet engines, fission and fusion nuclear power production, turbines for fossil power production, heat management systems and other leading edge areas of modern technology requires structural materials that are capable of withstanding fairly high mechanical stresses in adverse environments at temperatures of up to 1300oC. While, in many such cases, steels or intermetallic compounds can meet most of the requirements, poor creep resistance drastically narrows their areas of application. Even the best nickel-, iron-, and cobalt based superalloys retain their strength to only 900-1100oC, while many military and civilian needs require higher-temperature capabilities.

Thus, conventional high-chromium ferritic/martensitic steels were used for applications such as the first wall and blanket structure of a fusion experimental device, in coal or gas fired boilers and turbines in the power generation industry, and in many other machines, but their upper operating temperature is limited to 550-600°C. This limit has been relaxed by developing oxide dispersion strengthened (ODS) ferritic Fe-Cr-Al and ODS intermetallic Fe_3Al-based alloys, which are promising materials for high-temperature/high-pressure applications, due to the fact that they retain the best properties of high-ferritic steels (superior corrosion resistance in oxidizing, oxidizing/sulphidizing, sulphidizing, and oxidizing/chlorinating environments, resistance against irradiation swelling), but also possess extraordinary mechanical properties.

These alloys, with a typical composition of Fe-20Cr-5.5Al-0.5Y2O3 or Fe3Al-0.5Y2O3 (wt. %), are mechanically alloyed from constituent powders in a mill, and then consolidated by HIP, extrusion or rolling. These alloys contain sufficient aluminum to form an alumina scale (protective against an atmosphere or other aggressive environments), while the excellent creep properties are achieved by the incorporation of a fine dispersion of yttria particles, which often transform to yttrium-aluminum oxides over time. Present production methods lead to certain limitations upon ODS piece dimensions, in that they typically cannot be large. Fabrication of large parts, as well as complex shapes, needs a reliable method of joining ODS materials to themselves.

One of the most promising application of the ODS alloys is to very high-temperature heat exchangers, since they inherently require bonding of ODS tubes to each other. So, joining these materials is a very important task. However, one drawback with these alloys is the difficulty in bonding, which stems from several different reasons. One of the most widespread joining methods is brazing, which is not applicable to ODS alloys because the latter are used for their excellent strength. A brazing interlayer should possess the same high creep resistance. Materials with excellent strength and, simultaneously, sufficiently low melting points for brazing do not exist.

Another large group of bonding techniques is welding (arc, plasma, laser or electron beam). These processes are always accompanied by the local formation of a liquid phase, which inevitably results in a disturbed and coarsened oxide structure, which is unacceptable. It is considered essential that there is minimal disruption in the distribution or alignment of the yttria dispersion, since any changes would be expected to strongly influence the alloy microstructure and deteriorate the mechanical properties. Thus, in fusion welding of ODS alloys, the fine

dispersions of oxides agglomerate, leaving a joint which often has an order of magnitude lower high-temperature strength than the surrounding metal [1-4].

For the same reason, transient liquid phase (TLP) bonding did not provide a high quality joint – the fluid resulted in coarsening of the yttria inclusions and thus in low creep resistance. Additionally, the heat treatments associated with the TLP joining process were sufficient to remove any driving force for recrystallization for the bulk of the alloy, which also resulted in a decrease in the properties. So, only the solid-state joining techniques such as friction welding or diffusion bonding are suitable for joining ODS superalloys [5]. Agglomeration or coarsening of oxide particles may thus be avoided, and joints having mechanical properties that match the base material should be obtained.

Friction welding operations create fully-recrystallized grains of low aspect ratio at the joint centerline and substantially alter the oxide particle chemistry, dimensions, and shape in the joint region [6]. The resulting room-temperature and high temperature tensile strengths of joints were similar to those of the base material. However, the creep rupture strength of these joints was much poorer than that for the base material when tested in both longitudinal and transverse directions. Direct diffusion bonding also has been used to bond ODS superalloys [7], but neither cold strength nor creep resistance were measured. It is believed that, based on our experiments to implement direct diffusion bonding of MA-956 by hot pressing of the polished parts that proved to be unsuccessful due to a tenacious alumina scale, direct diffusion-bonding the ODS steels at temperatures below the melting point of the ODS alloys cannot result in a strong joint.

In another patent [8] it was proposed to bond ODS alloys by hot pressing (between two parts to be bonded) a powdered interlayer consisting of a nickel based alloy. The latter did not contain fine yttria inclusions, so that its creep resistance at temperatures over 1100^{o}C could not meet that for the ODS ferritic alloys. Also, diffusion bonding of iron-based steels by a nickel-based interlayer will inevitably result in intensive diffusion processes and interactions between the ferritic steel components and numerous interlayer ingredients, which would change the microstructure and decrease the mechanical properties. Unfortunately, none of the above-mentioned publications on solid-state bonding processes presented data on results for creep rate testing, so efforts to develop a reliable solid state ODS superalloy joining method must continue.

As shown in the SBIR Phase I project, this important task could be solved by plasma-assisted diffusion bonding. This method is a variation of a pulse-sintering technique, which has been successfully used for consolidation of numerous alloys, ceramics and composites (for instance, [9, 10]). Micro-plasma discharges between the surfaces being bonded appear during field-assisted joining, destroying surface oxide films and facilitating bonding. The pulse-sintering method has been successfully used to join ODS superalloy by consolidating of the particulate interlayer between two pieces being bonded [11]. This work was focused on the interlayer densification process, and no data on mechanical properties were presented. It is believed that if a strong and creep-resistant joint can be provided by direct plasma-assisted diffusion bonding, any interlayer (to be consolidated first and then to be bonded) is an unneeded complication.

During the SBIR Phase 1 investigation, alloy MA-956 and ODS iron aluminide were bonded, and the flexural strength of the joints obtained was measured. The best sample revealed a flexural strength value of 1675 MPa, which confirmed that plasma-assisted bonding can be used successfully to join ODS alloys.

Alloy MA956 is available commercially, which would allow rapid exploitation of a successful joining technique in production, for example, of heat exchanger tubes for very high-temperature operation. Although the resistance of MA-956 to degradation in sulfur-containing environments is less that that of ODS iron aluminide (Fe_3Al), its commercial availability and excellent properties make MA-956 the most promising alloy in the ODS family for demonstrating joining techniques. It is not unreasonable to expect that joining parameters developed for MA956 would be readily applicable to other ODS FeCrAl alloys. For this reason the TPOC approved a switch in the project focus from the ODS iron aluminide originally intended to MA956.

2. Procedure

2.1. Starting Materials

The program started by bonding MA-956 (originally available from Special Metals, Inc., of Huntington, West Virginia). Later, supply problems with MA-956 arose, due to Special Metals discontinuing regular production of MA-956 while under bankruptcy protection, so that purchasing of any amount of MA-956 smaller than 20,000 lb proved to be impossible. For this reason, MA-956 was replaced in later experiments by PM2000 (available from Metallwerk Plansee GmbH, Austria). This alloy has a very similar composition to MA956 (see Table 1), and possesses similar mechanical properties.

Table 1: Chemical Composition of ODS Ferritic Superalloys

Material	Chemical composition, weight %					
	Fe	Cr	Al	Ti	C	Y_2O_3
MA-956 [12]	74	20	4.5	0.5	0.05	0.5
PM2000 [13]	Bal.	19	5.5	0.5	-	0.5

For butt joining, MA-956 rods were used both the secondary-recrystallized, large-grained condition (as-produced by the manufacturer), and unrecrystallized (with a fine, sub-micron grain size). PM2000 for butt joints was only used in the unrecrystallized, fine-grained form. For one set of experiments MA-956 rods processed under different conditions (as shown in Table 2) and cordially provided by Dr. B. Kad, University of California at San Diego, were used. For tube joining, only as-produced, secondary-recrystallized (large-grained) PM2000 tubes and rods were used.

Table 2: Processing Conditions for MA-956 Rods

Batch #	Extrusion ratio	Extrusion temperature, ^{o}C	Annealing temperature, ^{o}C	Annealing time, h
A1A1A1	10 : 1	1000	1000	0.5
A1A1A2	10 : 1	1000	1000	1.0
A1A1A3	10 : 1	1000	1000	6.0
A1B1A3	10 : 1	1075	1000	6.0
A1B1A1	10 : 1	1075	1000	0.5
A1B1A2	10 : 1	1075	1000	1.0
A1C1A3	10 : 1	1150	1000	6.0
A1D1A3	10 : 1	1200	1000	6.0
A1C1A1	10 : 1	1150	1000	0.5
A1C1A2	10 : 1	1150	1000	1.0
A1D1A1	10 : 1	1200	1000	0.5
A1D1A2	10 : 1	1200	1000	1.0

2.2. Pulse-Sintering Machine

For the SBIR Phase II project, both the loading unit (with chamber) and the pulse unit (with power supply) were built anew, in order to provide an opportunity to implement plasma-assisted joining of samples of up to 1" OD and 2" length at temperatures up to 1400^{o}C and pressures up to 80 MPa (Figures 1, 2). Special software was developed to simultaneously monitor voltage, current, temperature (from both/either a pyrometer and a thermocouple), pressure, ram displacement, and oxygen content in the chamber against current or elapsed time.

2.2.1. Loading Unit

The loading cell consists of a vacuum chamber (1, (Figure 3), with a water-cooled ram (2), which also plays the role of a feed-through connector [pulsed electric current is supplied through an electrode (3)]. Since the chamber (2) is another electrode, it is insulated from the ram by the machinable ceramic bushing (4) and the double-lipped seal (5).

The samples being heated must not be allowed to be in direct contact with the water-cooled ram, since the latter would absorb too much energy. To avoid this, an intermediate ram (6) was introduced, which must tolerate high temperatures and yet possess low electrical resistance. The most suitable material for this purpose is graphite. The ram (6) should be, at the same time, sufficiently wide to decrease electrical resistance, tall to distant the sample from the water-cooled parts, and small to absorb as little heat as possible. The same conflicting requirements had to be reconciled in designing the support on which the sample (7) rests. The optimum dimensions of the graphite ram (6), graphite support (8), and copper support (9) were determined from numerous experiments.

Figure 1: **MER Pulse-Sintering Machine**

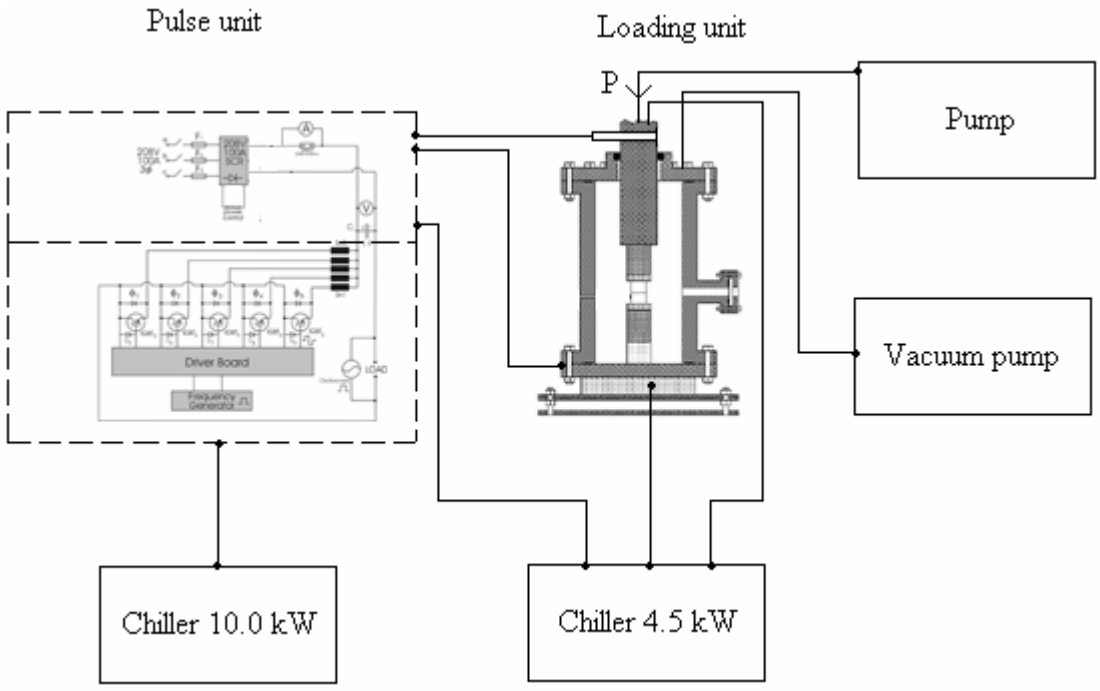

Figure 2: Pulse-Sintering Machine Scheme

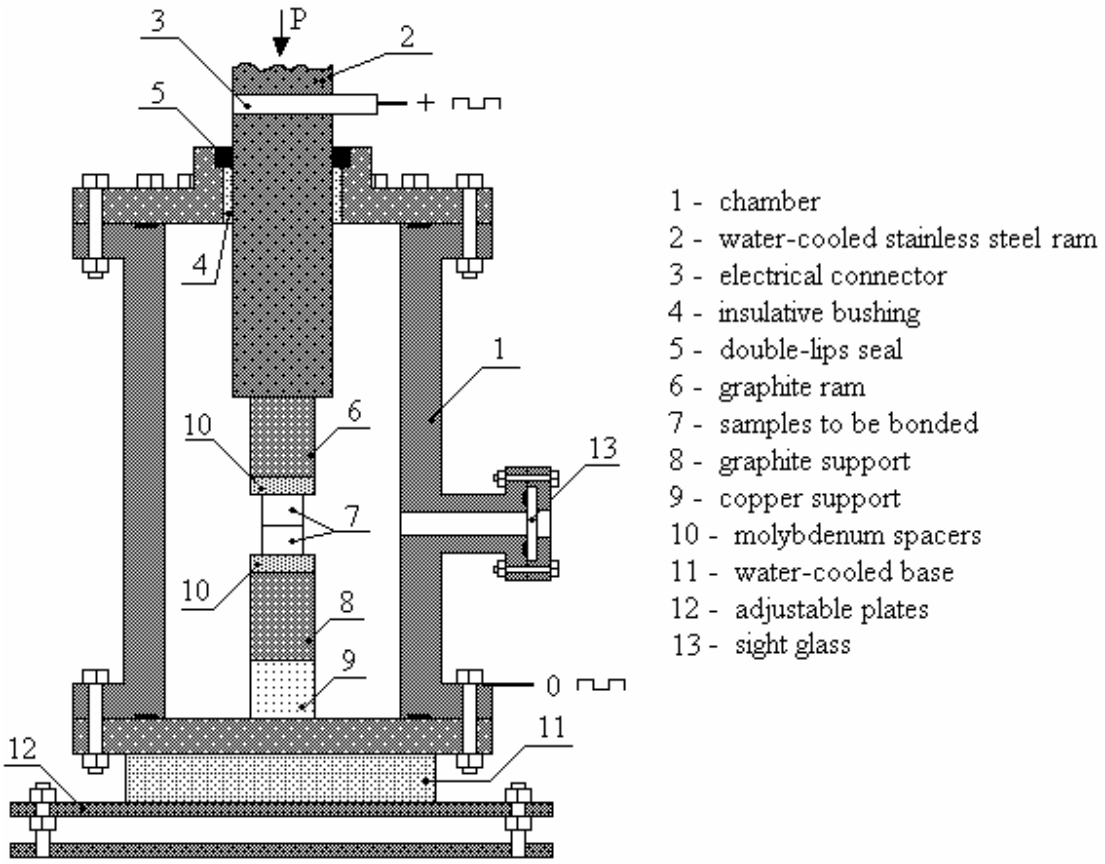

Figure 3: Scheme of Loading Unit (Chamber) of Pulse-Sintering Machine

Since iron enters into a eutectic reaction with carbon at 1147°C, so that iron-based materials must not touch graphite at temperatures above this eutectic value. In order to prevent the samples from melting at the joining temperature, thin molybdenum plates (10) were placed between the sample and the graphite pieces. Also, since too much heat was being transferred from the samples down to the chamber, the latter was provided with a water-cooled base (11). During joining, the axis of the ram (2) must be perpendicular to the surfaces being bonded. In order to line up the samples relative to the ram axis, the chamber was installed onto the adjustable plates (12). The temperature is measured through a sight glass (13) by a two-beam, infrared, optical pyrometer with digital output.

The chamber may be operated in both vacuum and inert gas atmosphere. Oxygen content in the gas is controlled by a Model 60 oxygen sensor (Advanced Micro Instruments, Huntington Beach, CA). Ram displacement was measured with a Mitutoyo micrometer. Temperature was measured with a two-beam model 99C15-002 infrared pyrometer (IRCON, Niles, IL). Pressure was measured by an ECO-1 transducer (WIKA, Germany). All measuring instruments provided digital outputs.

2.2.2. Pulse Unit

The high-current pulsar consists of two parts (Figure 4): a high-current power supply, and a high-speed switch. Two commercially-available, multipurpose DC-1500 (Lincoln Electric, 480 V / 1500 A DC) welders were used as power supply for the pulsar unit.

The high-speed switch contains an INSTEK, model GFG-8216A (Goodwill Instruments, Malaysia) frequency generator with a TTL output signal registered by a two-channel digital real-time oscilloscope TDS-210 (Textronix, Beaverton, OR). The generator can be tuned for different frequencies and duty cycles. The TTL signal from the frequency generator is routed to a driver board, which splits the input from the generator into five outputs – one for each IGBT transistor.

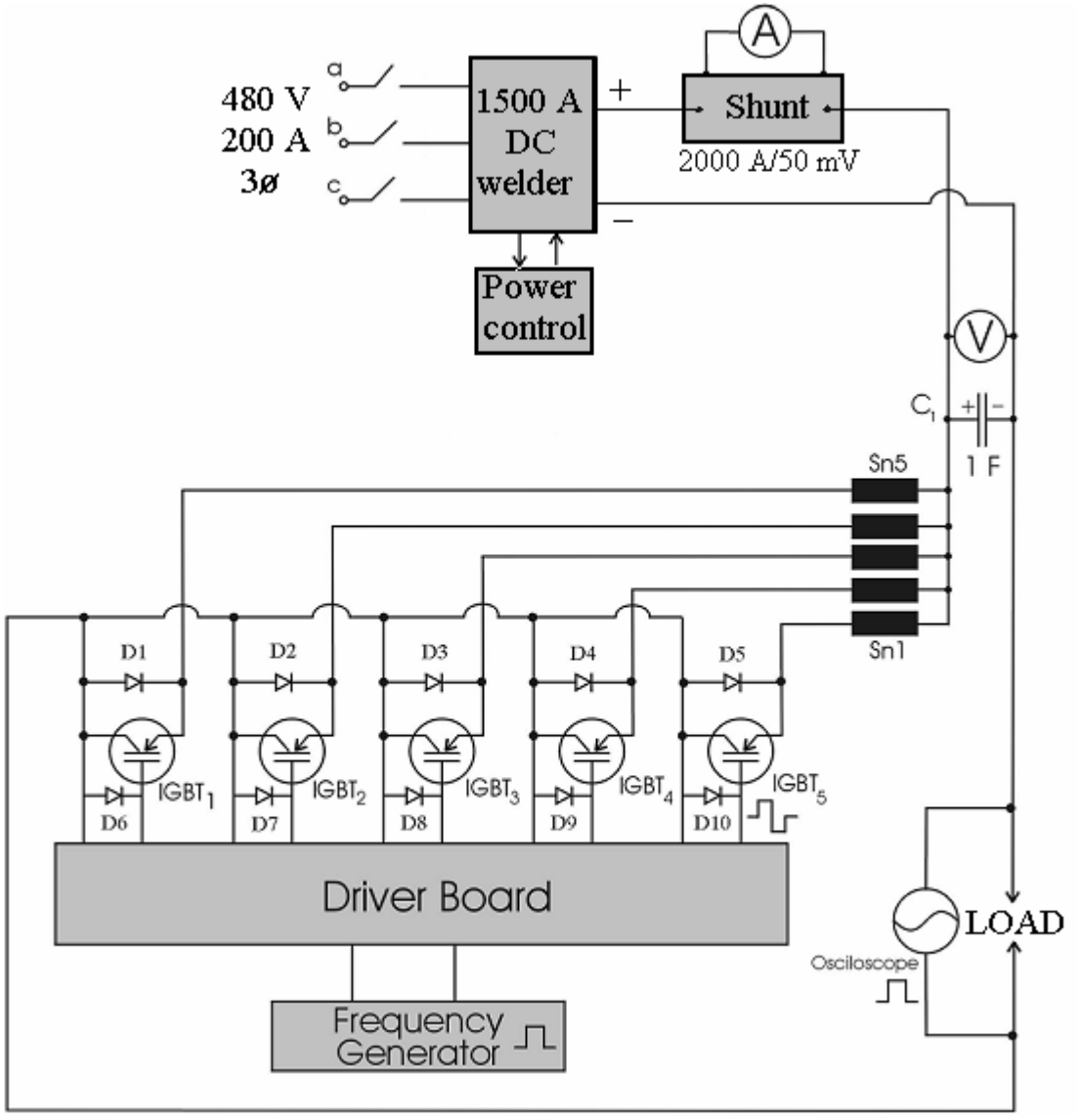

Figure 4: Pulse Unit Electric Schematic

The high-speed switcher is based on five IGBT transistors connected in parallel. Each transistor is provided with its own snubber system, which protects them from destroying back current flow. The output signal from the driver board switches the IGBT transistor ON/OFF. This signal has the same frequency and duty cycle as the generator, but a different (TTL) configuration. The IGBT transistor is designated to be forced ON by applying +12 V to the gate, and to be forced OFF by applying -10 V to the gate. Thus, while the TTL signal from the frequency generator has a 0/+5 v output, the output of the driver board must be +12 V / -10 V.

Each IGBT possesses slightly different parameters, and so they cannot match exactly when connected in parallel. Therefore, each IGBT transistor is provided with another (output) snubber (Sn1-Sn5, Figure 2). These snubbers, by acting together, ensure matching of the different IGBTs. The amount of energy being evolved in the transistors during their work can easily result in overheating, unless precautions are taken. In order to maintain the temperature of the transistors below 70^{o}C, they are situated on a water-chilled heat sink cooled by a 10 kW chiller.

All the signals from the generator and control circuits for the transistors are low current. Field-assisted joining requires high-current pulses to form micro arcs at the interface facilitating joining. In order to create powerful electric pulses, a block of capacitors with a total capacitance of 1 f is used. The generator produces the TTL signal which controls IGBT transistors that, in turn, control the power capacitors ON/OFF current in accordance with the preset frequency and duty cycle. This DC power supply provides a fairly “dirty” output (the parameters of this signal are not sufficiently stable). This deficiency is corrected by the block of capacitors, which works as a very fine filter to smooth the power supply output. Since the high-current pulsar design, as constructed, is not of a resonance type, it provides an opportunity to change frequency from 0 to 10 KHz. and duty cycle from 10 to 100%.

2.3. Bonding Procedure

Alloy MA-956 or PM2000 pieces 0.5-0.75” OD x 0.25” thick (for metallography) or 1” tall (for mechanical testing) were ground (on both sides) and polished (on one side) by successively finer silicon carbide sandpapers (ending with 1200 grit) to obtain a roughness of 5 microinches. The grinding/polishing procedure provided parallelism of the faces of ±0.001”. The pieces were cleaned in an ultra-sonic bath containing acetone, then in ethanol, and finally were assembled in the pulse-sintering machine chamber. Special removable centering adjustments were used to line up the pieces to be bonded with the press ram (the samples axis must be in line with that of the ram) in order to prevent premature bending or destruction of the samples. Pressure was transferred through the graphite spacers. As described above, 1 mm (0.040”)-thick molybdenum foil was placed between the samples and the spacers in order to prevent melting during bonding.

Plasma-assisted joining was performed in an argon atmosphere. The oxygen content of the gas was maintained so as not to be greater than 0.2%. An initial bonding pressure was applied in order to provide a reliable electric contact between all parts, and to prevent arcing and melting of the samples. The voltage and current applied depended on sample dimensions (which could vary), and the power output was set by the operator. Numerous experiments resulted in

determining the optimum parameters for pulse heating. An output current of 1200 A (at 6 V) was used at a 63 Hz frequency and 70% duty cycle. Under these conditions, a 1" in diameter, 2" long MA-956 alloy rod was heated to 1200^{o}C for ~1 hour. Short (0.5" in diameter) MA-956 pellets (for metallography) were heated to the same temperature for ~10 minutes. The above-mentioned values of frequency and duty cycle were used in all the experiments of the current project.

After bonding the joined pieces were cut for mechanical testing, and polished for optical metallography or SEM/EDS investigations.

2.4. Post-Bonding Characterization

For metallographic examination, the samples were polished with silicon carbide paper and etched by swabbing with a solution of 40 ml HCl + 10 ml HNO_3 + 10 ml lactic acid + 15 ml H_2O. SEM and EDS analyses were carried out using a field-emission Amray 1860 microscope with IXRF model 500 X-ray Optics Detector, and EDS 2004 Version 1.3 software. TEM specimens were cut from the samples using a Hitachi SB2000A focused ion beam (FIB) instrument operated with a 30kV beam of Ga ions, and TEM micrographs were taken on a Hitachi HF2000 microscope operated at an accelerating voltage of 200kV.

Cold flexural test was carried out in accordance with ASTM E 290 (the free bend test). This is a standard test method for bend testing of materials for ductility. It does not characterize the strength of ductile steels like MA-956 since during testing a ductile material bends without breakage. However, this works differently for the bonded bars. If a joint is not good enough, it breaks during the bending test. In the current project ASTM E 290 was used for quick characterization of some joints (whether the latter formed or not under certain processing parameters).

Hot tensile test was performed at Oak Ridge National Lab (ORNL) at a very low loading speed, which, as stated by the ORNL specialists, allowed evaluating creep resistance. The ORNL hot ultimate tensile strength (UTS) sample blueprint is presented in Figure 5a. In order to observe the microstructure of the samples to be mechanically tested, a segment was cut off on the periphery of the sample, polished and investigated by SEM/EDS. The main portion of the sample was used to extract the "dog bones" for tensile tests as shown in Figure 6. High-temperature creep testing was performed at Stork-Herron Testing Laboratories (Cleveland, OH) and at Westmoreland Mechanical Testing & Research Lab (WMT&R) (Youngstown, PA). A Stork-Herron creep sample is shown in Figure 5b. The WMTR sample blueprint is given in Figure 7a. In this case small pieces were also cut off the middle of the bonded rods for EDM/EDS investigation so as not to disturb the gauge of the creep testing sample (Figure 7b).

3. Plasma-Assisted Bonding ODS Superalloys: Butt Joint

3.1. Bonding Recrystallized ODS Superalloys

Commercially-available recrystallized (large-grained) ODS superalloy MA-956 rods were bonded at 1150-1270^{o}C in an argon or argon + 5% hydrogen atmosphere under 30 MPa / 5 ksi to 90 MPa / 13 ksi pressure. The joining conditions for each sample are listed in Table 3.

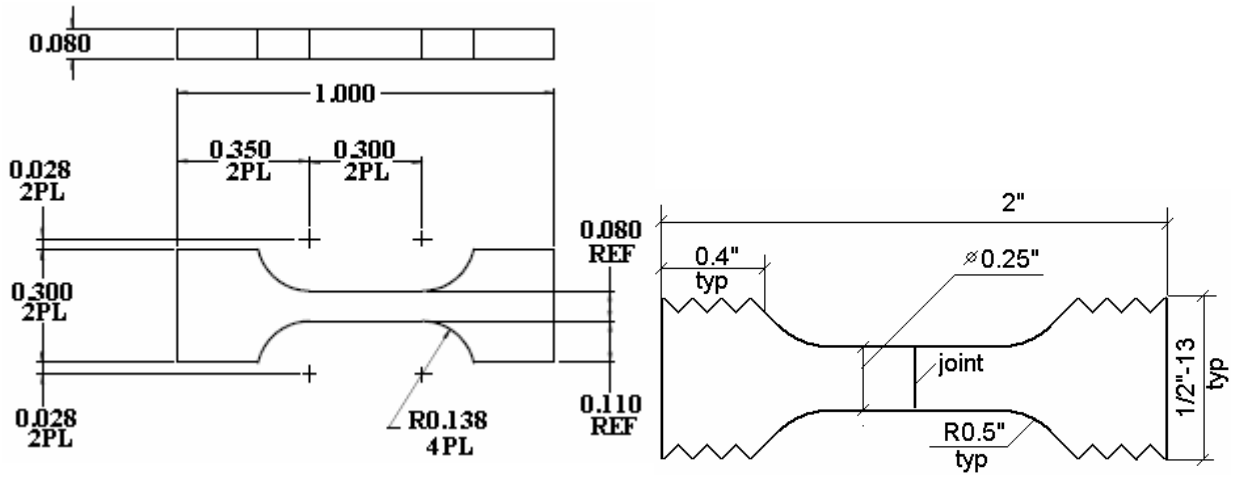

Figure 5: Samples for Mechanical Testing
a - ORNL Hot Tensile Test "Dog Bone"; b – Stork Herron Hot Tensile Test Sample

Table 3: Bonding Parameters for Recrystallized MA-956

Designation	Bonding				Change in shape
	Temperature, °C	Pressure, MPa / ksi	Time, Min	Atmosphere	
MA-29	1100	30 /4.3	60	Ar	
MA-30	1100	50 / 7.2	60	Ar	
MA-31	1100	80 / 11.6	60	Ar	
MA-16	1100	90 / 13.0	60	Ar	Oblate
MA-15	1150	50 / 7.2	5	Ar	
MA-14	1150	50 / 7.2	60	Ar	
MA-7	1150	70 /10.1	60	Ar + 5%H_2	
MA-35	1150	80 / 11.6	60	Ar	Distorted
MA-9	1200	50 / 7.2	60	Ar + 5%H_2	
MA-38	1200	80 / 11.6	60	Ar	Distorted
MA-8	1200	[#]90 / 13.0 → 70 /10.1	60	Ar + 5%H_2	Oblate
MA-10	1270	50 / 7.2	60	Ar + 5%H_2	
MA-37	1270	80 / 11.6	60	Ar	Distorted

[#]Starting pressure was 90 MPa / 13.0 ksi, but was reduced to 70 MPa / 10.1 ksi to avoid further plastic deformation of the sample.

The first set of runs was carried out in an argon + 5% hydrogen atmosphere. This set had the goal of establishing the optimum bonding temperature and pressure. There is a stress-temperature threshold condition above which the ODS superalloy will revert from exhibiting high creep strength to rapid deformation. If this threshold is exceeded, the sample fails in compression during bonding. Thus, at a given temperature, a series of samples was bonded at progressively higher pressures, until noticeable distortion occurred. Thus, the maximum pressure, at which the sample could be joined without significant changes in dimensions, was established.

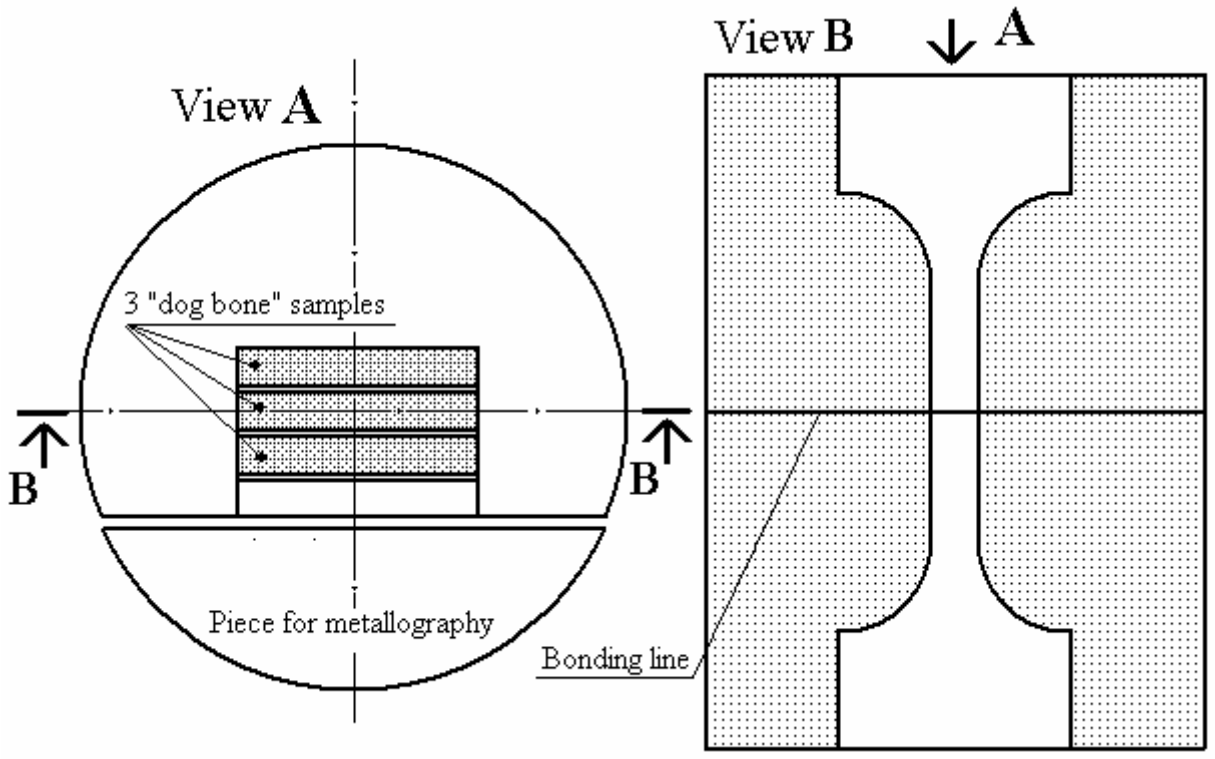

Figure 6: ORNL High Temperature Tensile Test Sample Locations in Bonded Rods

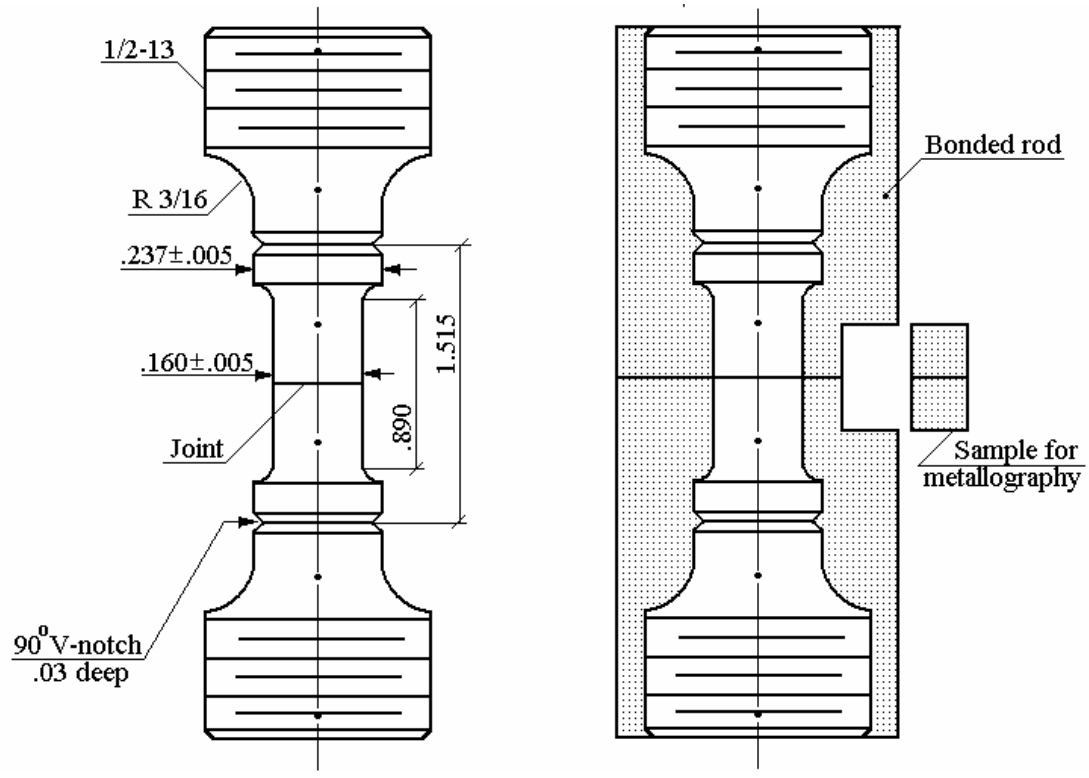

Figure 7: WMTR Creep and Hot Tensile Test Sample (a) and its Location in Bonded Rod (b)

It has been reported [5] that, at a bonding temperature of 1100°C, noticeable deformation of alloy MA956 starts at 72 MPa /10.4 ksi. In our experience, recrystallized MA-956 can be bonded at 1100°C and 80 MPa / 13 ksi with negligible distortion. For 1150°C the maximum pressure at which (essentially) no distortion was observed was 70 MPa / 10.1 ksi, at 1150°C; 60 MPa / 8.7 ksi at 1200°C; and 50 MPa / 7.2 ksi at 1270°C. If the pressure threshold for each temperature is exceeded, the microstructure changes drastically (Figure 8). Segregation and coarsening of the alloying phases occurs resulting in a drop in high-temperature creep resistance. Another reason for a decrease in mechanical properties is seen in the formation of multiple longitudinal cracks along the grain boundaries between the large recrystallized grains (Figure 9) of the sample MA-37, which was overloaded at 1270°C.

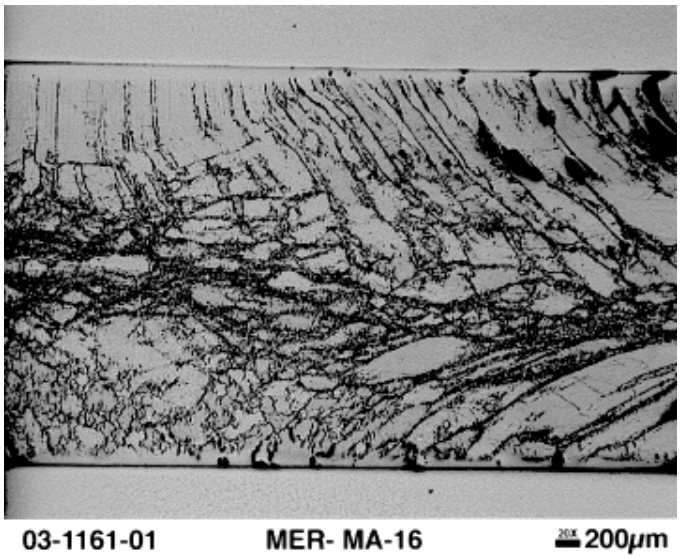

MA-8 1200°C 90 MPa / 13 ksi 60 min

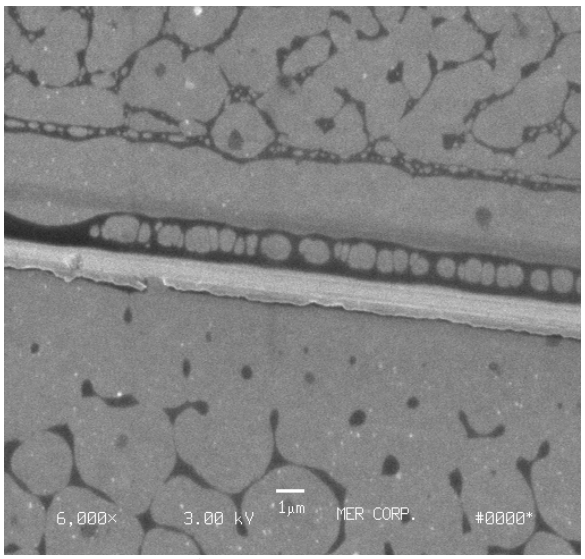

MA-16 1100°C 90 MPa /13 ksi 60 min

Figure 8: Microstructure of Bonded Samples Overpressed during Joining

The obtained joints did not contain visible pores or cracks (Figure 10). However, the microstructure did not remain undisturbed. Sometimes, the joint was barely visible in unetched samples (Figure 10b). In other cases, the joints were decorated with a chain of white inclusions (Figure 10a) that were much coarser than the original oxide dispersoids in MA-956. An increase in temperature and pressure (while the sample was not distorted) did not result in noticeable changes in the microstructure. Sometimes, black-appearing, round inclusions [which are plentiful in the bulk material (Figure 11)] were found to enrich the joint (Figure 10d), suggesting intense diffusion of the alloying phase(s) from the sample bulk to the joint area.

SEM analysis of the same etched samples showed that, in most cases, plasma-assisted bonding of recrystallized MA-956 did not result in grain growth across the joint, although sometimes there was an obvious match between the grains of two bonded halves (Figure 11a, marked by arrows). During recrystallization by the manufacturer, grain growth had already taken place to the fullest extent, so that no small grains remained in the material and, hence, there was no driving force for secondary recrystallization and for growth of grains across the joint.

Figure 9: Macrostructure of Bonded Sample Overpressed during Joining

It is seen in Figure 11 that, within the investigated range, bonding temperature, pressure and dwelling time did not noticeably affect the microstructure, which contained round, black inclusions of less then 1 μm size, both in the bulk material and at the interface, with the latter sometimes being enriched with those inclusions (Figure 11d-f). EDS analysis indicated that all black inclusions contained titanium (Figure 12), while some contained Ti+Al or Ti+Y, and a very few contained Ti+Al+Y. The bonded interface obviously was enriched with all three alloying elements. The oxygen content in the joint was greater than that for the bulk material, while most of the inclusions did not contain oxygen at an above average level. This was considered to be surprising, because MA-956 is mechanically alloyed with yttria, and the areas enriched with Y should also contain O. It was supposed that coarsening of fine oxide grains occurred due to an excessive dwell time during bonding. However, sample MA-15 which had a joining dwell time of only 5 min. contained the same black inclusions (Figure 11f).

The first runs were carried out in an Ar + 5%H_2 atmosphere. A run was performed in an atmosphere of pure argon to determine any effects of hydrogen used in the initial runs on the composition of the Y_2O_3 particles and hence the alloy microstructure. The latter did not change even a little (Figure 11e). It is worthy of note that the grain boundaries that were located parallel with the pressing direction (and perpendicular to the joint), were totally depleted of yttrium, while the interface and the linear defects that were parallel to the joint (and perpendicular to the pressing direction) were very much enriched by yttrium.

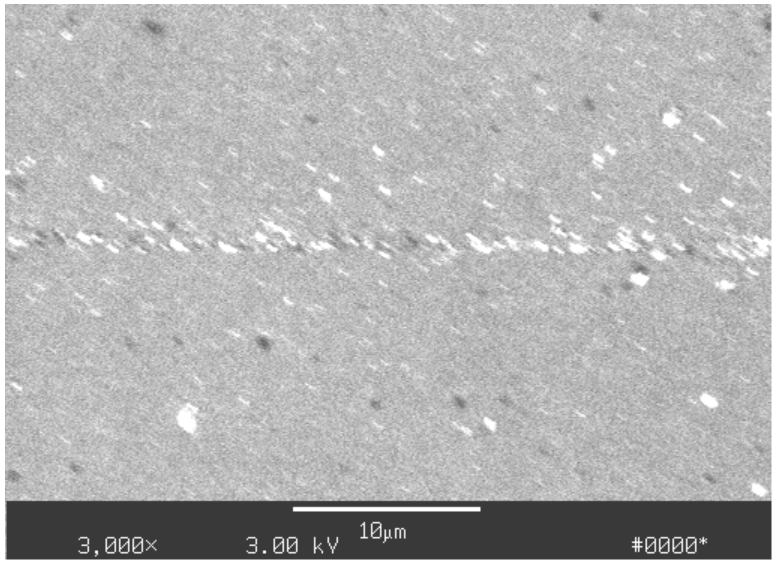

a) MA-7 1150°C 70 MPa / 10.1 ksi 60 min

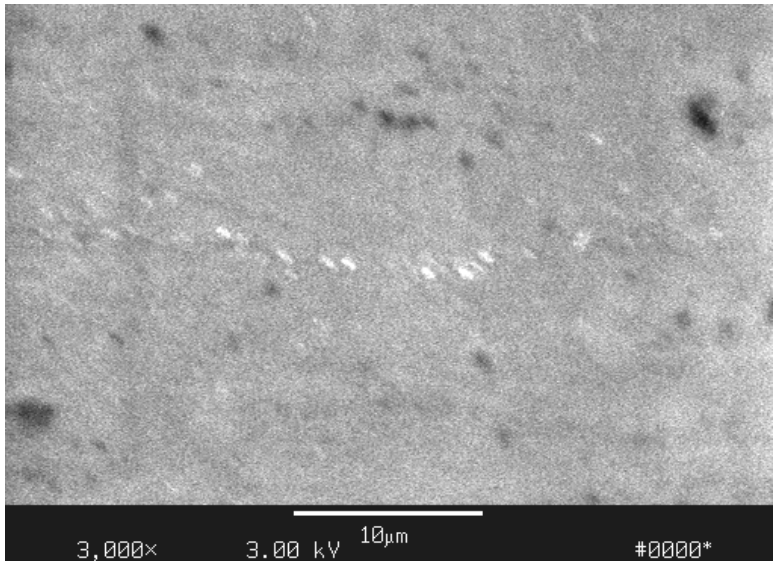

b) MA-7 1150°C 70 MPa / 10.1 ksi 60 min

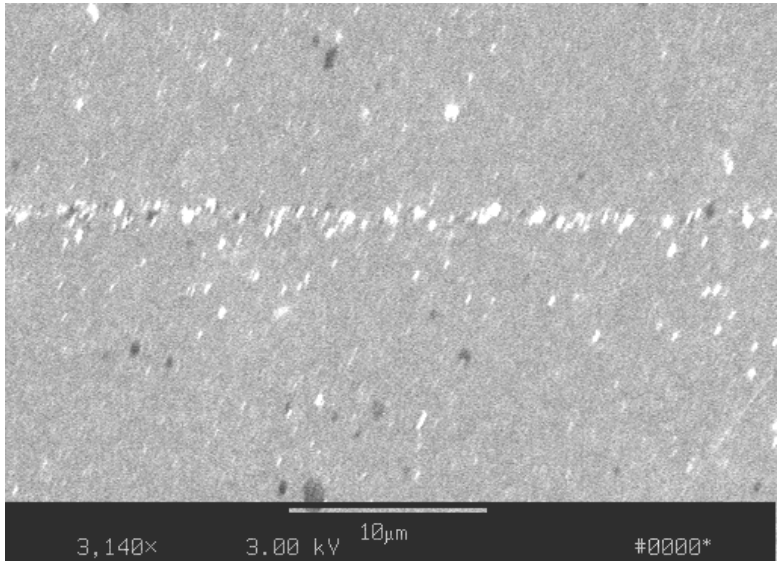

c) MA-9 1200°C 50 MPa / 7.2 ksi 60 min

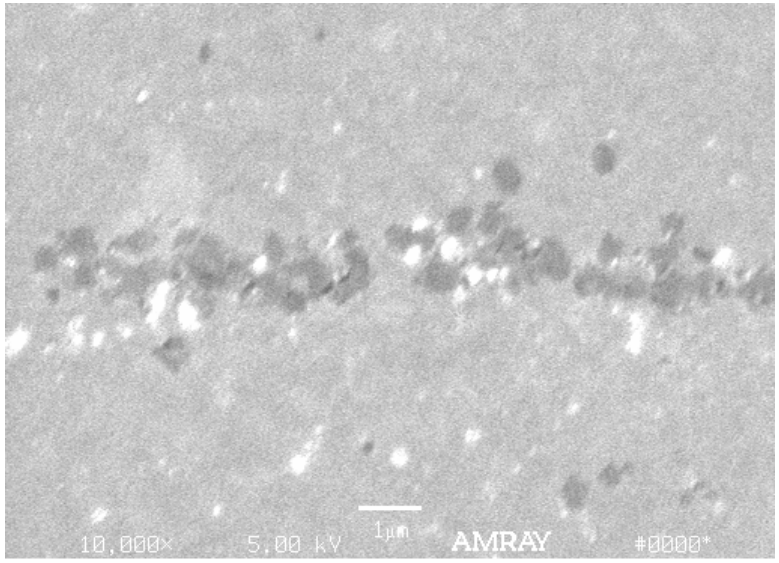

d) MA-7 1270°C 50 MPa / 7.2 ksi 60 min

Figure 10: Microstructure of Bonded Unrecrystallized MA-956 (unetched)

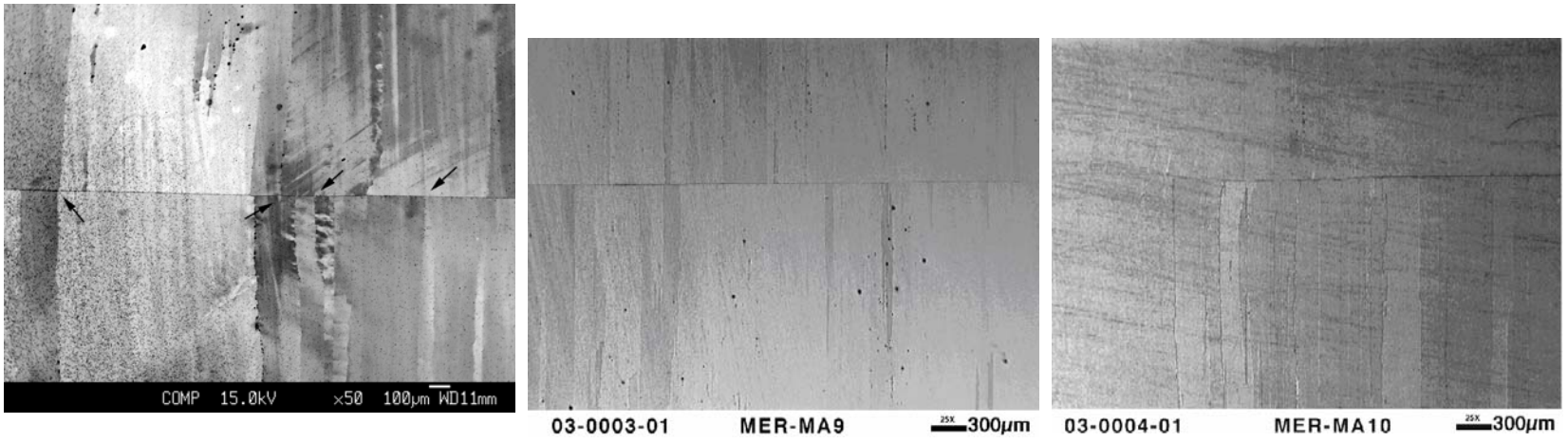

a) MA-7 1150°C, 70 MPa, 60 min, Ar+H_2 b) MA-9 1200°C, 70 MPa, 60 min, Ar+H_2 c) MA-10 1270°C, 70 MPa, 60 min, Ar+H_2

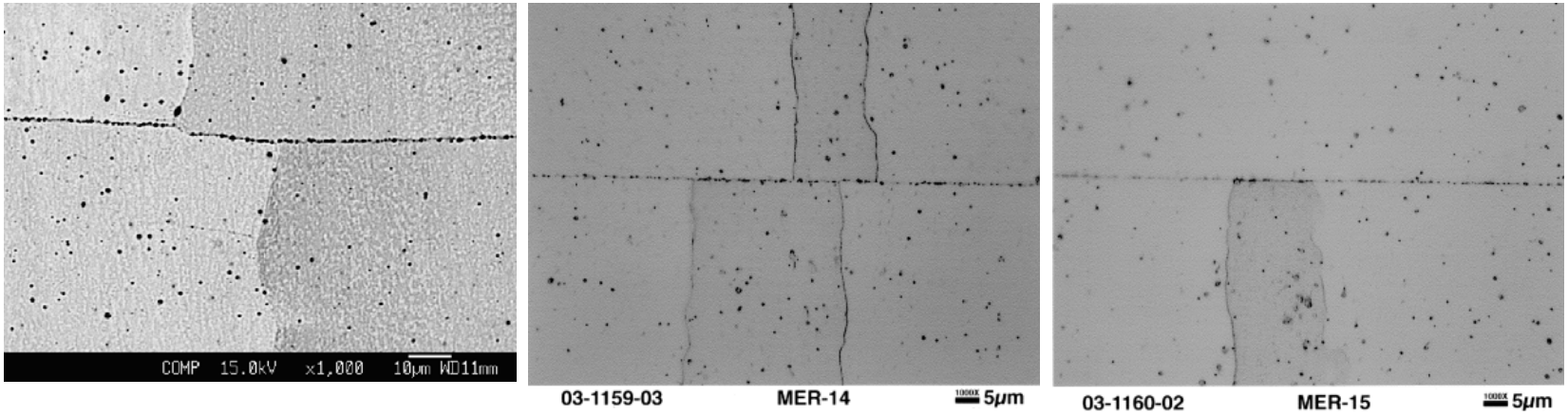

d) MA-7 1150°C, 70 MPa, 60 min, Ar+H_2 e) MA-14 1150°C, 70 MPa, 60 min, Ar f) MA-15 1150°C, 70 MPa, 5 min, Ar

Figure 11: Microstructure of Bonded Unrecrystallized MA-956 (etched)

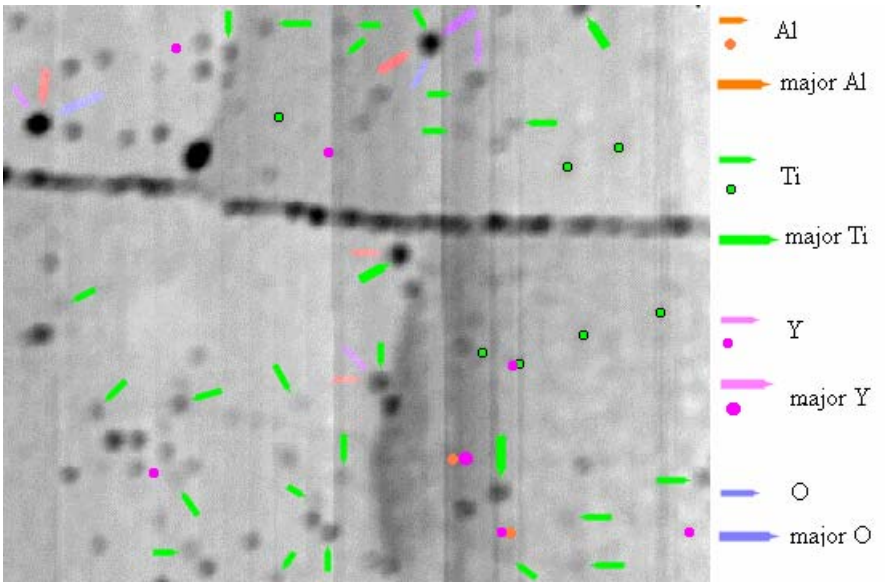

a) Base Image for Mapping (Elements are Marked by Colors)

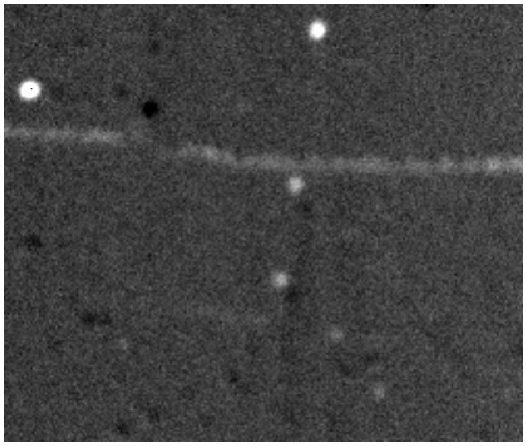

b) Aluminum

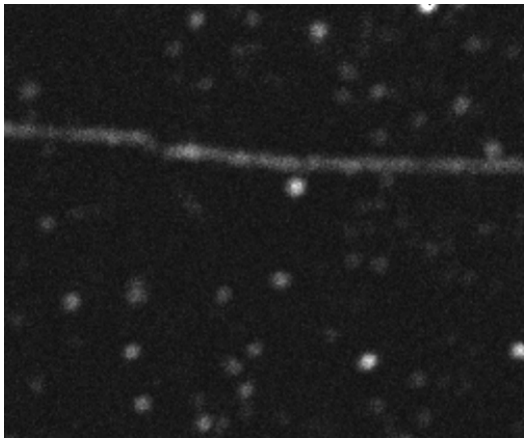

c) Ti

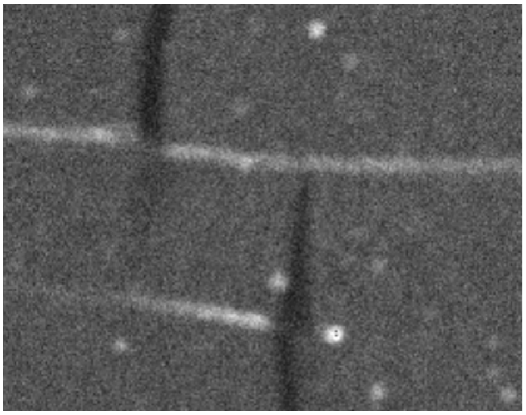

d) Yttrium

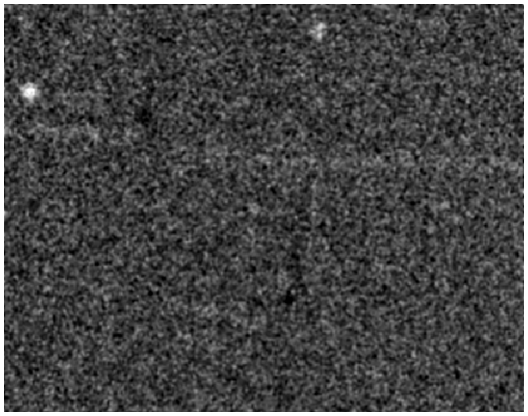

e) Oxygen

Figure 12: EDS Mapping of Sample MA-7 (1150^{o}C, 70 MPa, 60 min, Ar+5%H_2)

More detailed investigation of the joint microstructures bonded by pulse-sintering was carried out at ORNL using TEM (Figure 13). The inclusions at the interface were found to consist of alumina, yttrium-aluminum garnet (YAG), and/or titanium carbide. The inclusions were often situated in pores between the two halves being bonded, and appeared to be preventing the surfaces from joining in those locations. Other inclusions of a different type were the columnar alumina particles (similar to those observed in [5]) that formed a continuous tenacious layer on the surfaces being bonded. ODS alloys cannot be diffusion bonded at temperatures greater than the alloy melting points, which are too low to cause sintering of alumina. Thus, alumina scale, stand-alone inclusions, and columnar alumina particles cannot be bonded to themselves at the bonding temperatures used. These inclusions also block contact of the bulk material, thus preventing bonding.

Creep testing of samples MA-29, 30, 31 and 34 was carried out at WMT&R. The results were poor, due to the reason explained in the previous Section. In order to eliminate this cause of failure, it was necessary to implement an approach proposed by Dr. I.G. Wright (ORNL): secondary recrystallization across the bonded interface during bonding of unrecrystallized ODS alloy. If grain growth can occur across the joining line, the oxide-oxide contacts at the joint may be isolated and no longer constitute a plane of weakness.

3.2. Bonding of Unrecrystallized ODS Superalloys

3.2.1. Bonding Unrecrystallized ODS Superalloys without Post-Bonding Heat Treatment

Recrystallization following joining of an unrecrystallized ODS alloy could be ensured by heat treatment after bonding, or recrystallization could take place in-situ during plasma-assisted bonding (if the processing temperature and dwell time were appropriately chosen for recrystallization to occur). The set of experiments described in this chapter was devoted to the second variation: recrystallization during bonding, with no requirement for a post-bonding heat treatment.

As mentioned above, implementation of this project work plan occurred under extreme shortage of the starting material – commercially-fabricated ODS MA-956. As a result, experimentation in this portion of the project used MA-956 rods produced by in a different project led by Dr. B.K. Kad at University of California at San Diego. The processing conditions for those rods are given in Table 2. Unfortunately, the rods to be bonded were produced under a range of different conditions, which could substantially influence the mechanical properties. The results obtained at this stage allowed the determination of the temperature-pressure range in which bonding occurred without plastic deformation that resulted in macro- and microstructural changes and a reduction in mechanical properties. These results were used subsequently as a basis for optimization of the processing of unrecrystallized ODS FeCrAl with reasonably-reproducible properties.

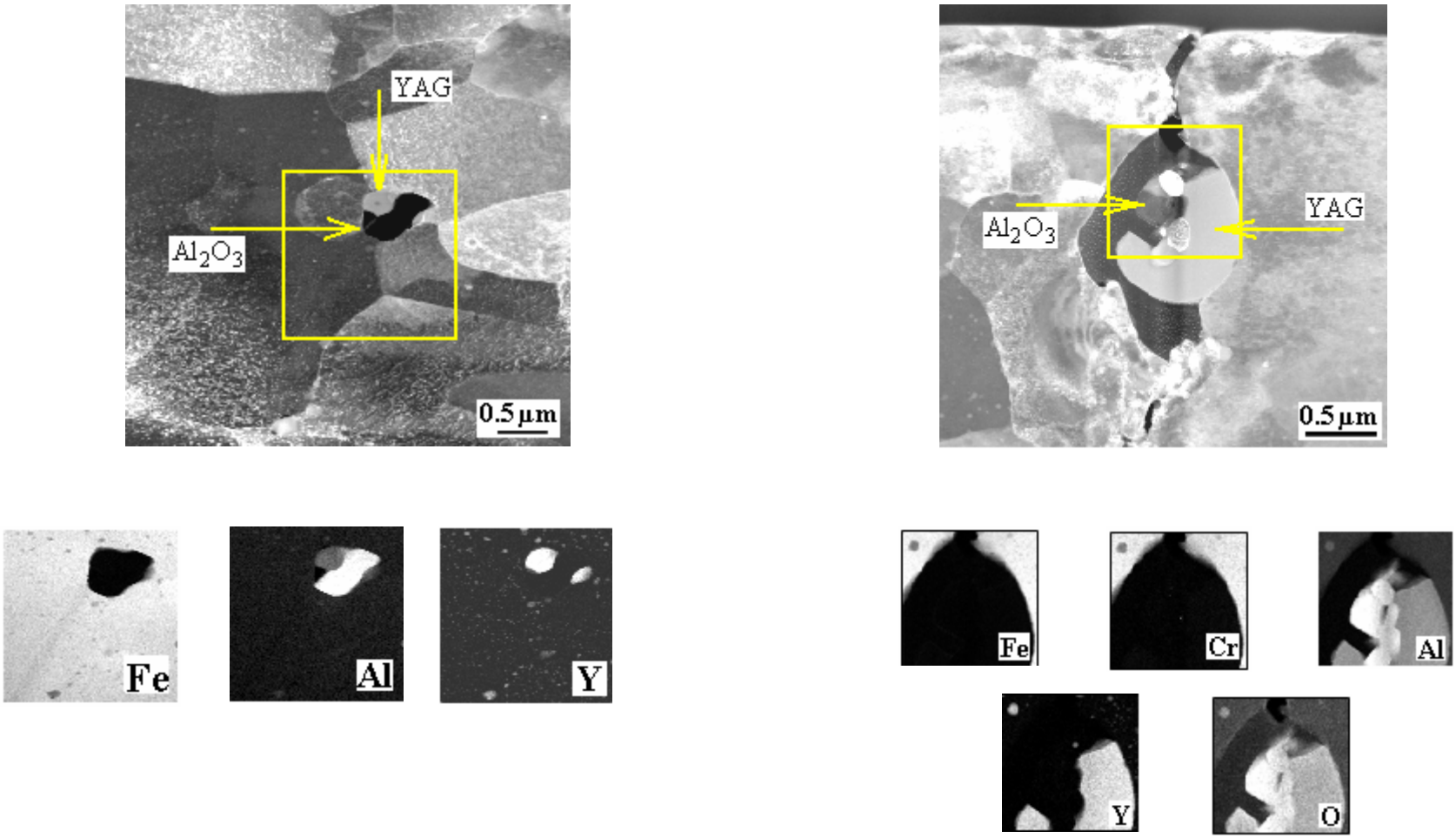

Figure 13: Phase Composition of Inclusions in Recrystallized MA-956 after Bonding

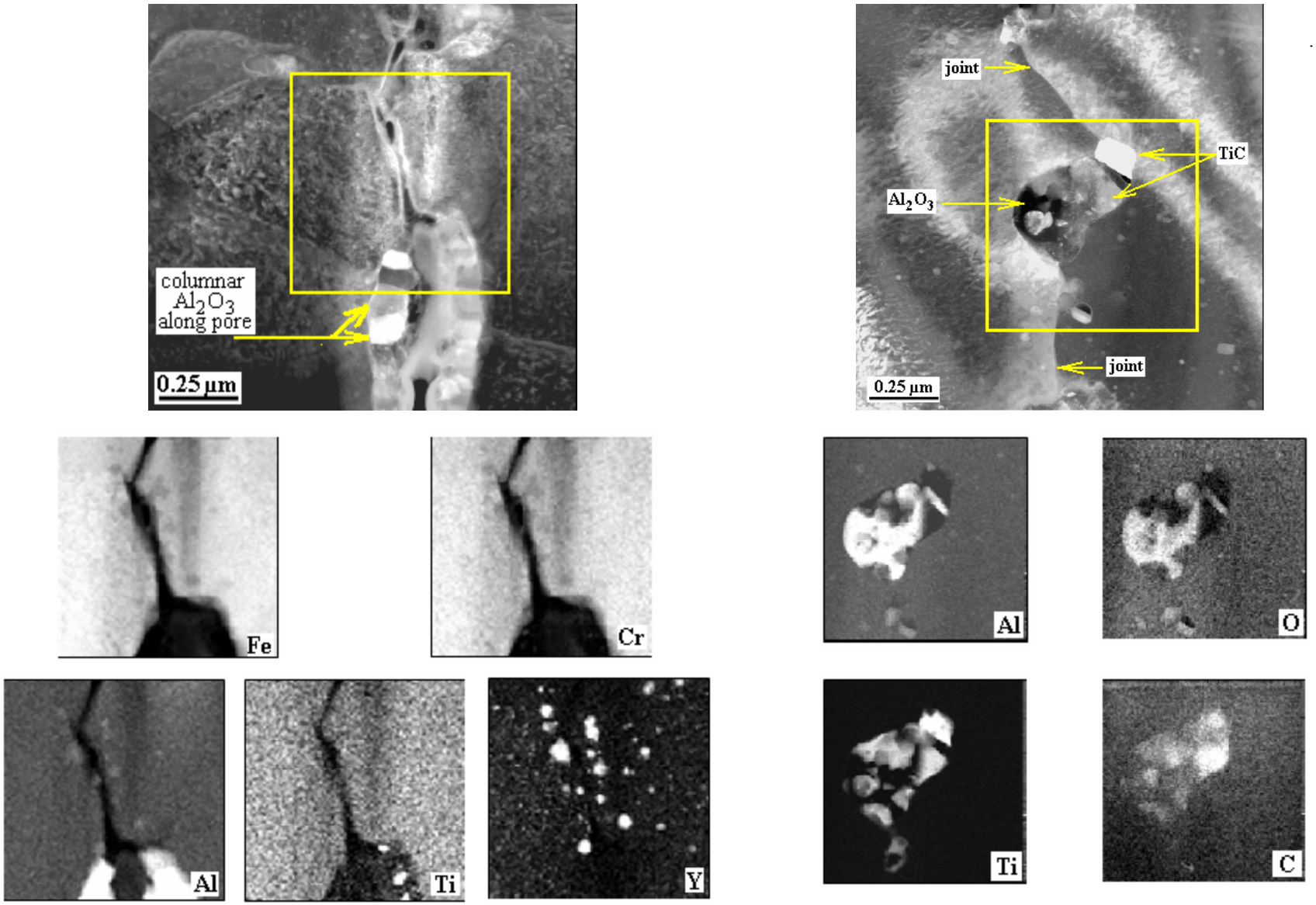

Figure 13 (cont-ed): Phase Composition of Inclusions in Recrystallized MA-956 after Bonding

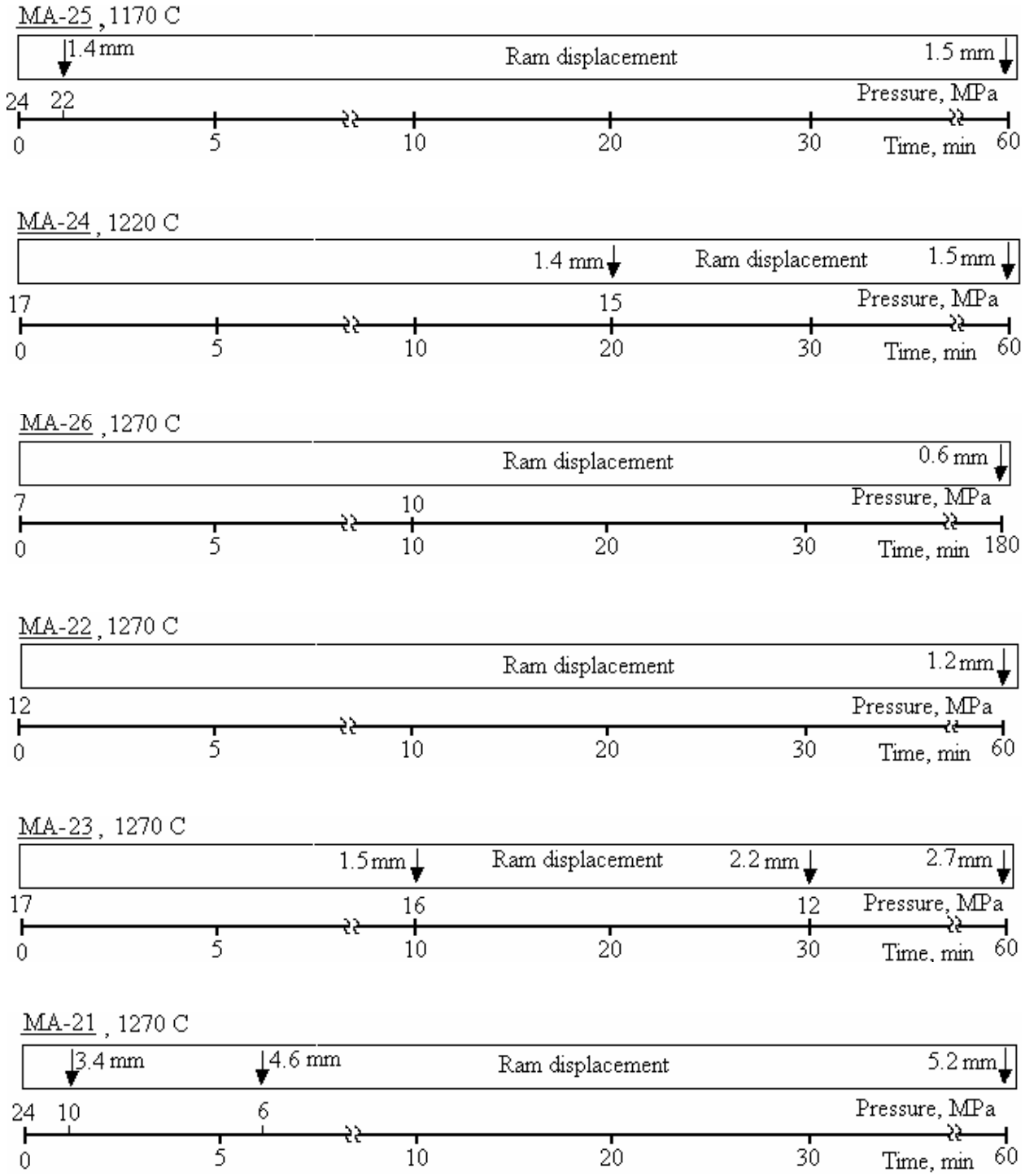

Figure 14: Bonding Parameters for Unrecrystallized MA-956

The samples were bonded as described in Section 2.3. The detailed information for each run is presented in Figure 14, which discloses the pressure and absolute downward movement of the ram (which is equal to the decrease in the sample length due to creep) at a certain temperature and time during a run. In this set of experiments, the runs started at high pressure. If during the dwell time the indicator measured a noticeable ram displacement (evidencing that plastic deformation had started), pressure was decreased until the ram stopped moving down. When recrystallized MA-956 was bonded, it was found (Section 3.1.) that, at each bonding temperature, there was a maximum pressure above which unacceptable, irreversible changes in the microstructure of the bulk material took place.

Obviously, the samples should be joined at a lower pressure than their compressive strengths at the bonding temperature used. As seen in Figure 15, at 1270°C the samples bonded at 16 MPa / 2.3 ksi and greater were distorted, while at lower temperatures even 25 MPa / 3.6 ksi did not result in noticeable dimensional changes and/or loss of shape. The joined rods of 19 mm (0.75") OD were cut with EDM into flat specimens in accordance with a scheme presented in Figure 16. Flexural testing at MER, high-temperature (at 900°C) 'slow-tensile tests' at ORNL, and high-temperature (at 1000°C) creep testing were performed to characterize the quality of the joints. For each type of testing, only a specimen chosen from a position (specified in Table 4) consistent in all the bonded samples was used.

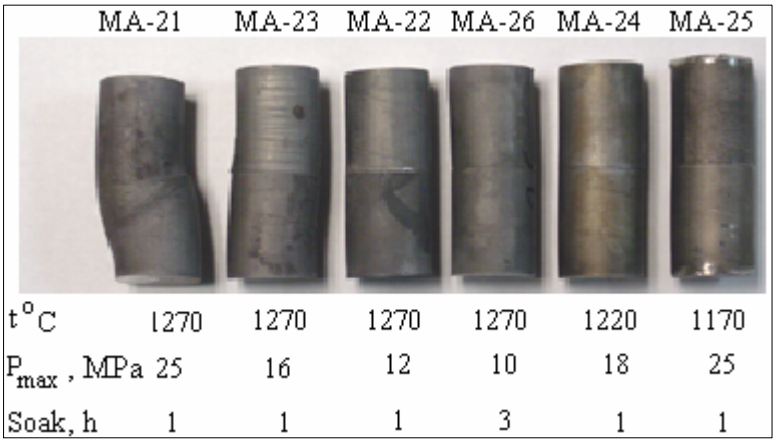

Figure 15: Samples Shape after Bonding under Different Conditions

The dependence of change in length on the maximum pressure applied was close to linear (Figure 17). The experimental results showed that, at 1270°C and even at the small pressure of 10 MPa / 1.4 ksi, a small amount of creep occurred. Initially-applied excessive pressure dramatically increased the creep rate, even if the pressure was significantly decreased shortly thereafter. Thus, during experimental run MA-26, 10 MPa caused only a 1.2% decrease in length for 170 min whereas during run MA-21 the same pressure resulted in 2.4% creep during only five minutes. This happened because, in the latter run, a much greater pressure of 25 MPa / 3.6 ksi was initially applied which caused cracks, changes in microstructure and, ultimately, weakening of the material.

Before carrying out expensive testing at high temperatures, the cold flexural strength of the bonded samples was measured in order to confirm that joining had occurred. During this flexural test, the sample processed at 1270°C and the maximum pressure of 25 MPa / 3.6 ksi showed the lowest strength, and broke at the interface. The sample processed at 1170°C also broke at the interface, although at significantly higher stress. All the other samples did not break at all. They were bent uniformly at approximately the same stress until their median points touched the bottom fixture (Figure 18). This meant that the strength of the joints was at least not less than

that of the bulk material. For all the samples, the maximum stress was low, but this is a property of the bulk material, rather than being due to the joints obtained by the plasma-assisted process. A typical loading diagram for the cold flexural test is presented in Figure 19.

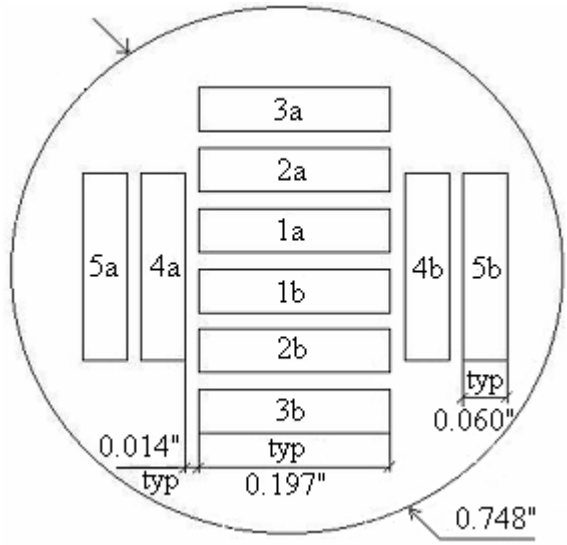

Figure 16: Specimen Locations in Unrecrystallized MA-956 Bonded Rods

Table 4: Specimens Positions in Bonded

Specimen position	Kind of testing	Testing company
2b	Flexural	MER
1a, 1b, 2a	Tensile, 900°C	ORNL
4b	Creep, 1000°C	Stork-Herron

Neither for the cold flexural test, nor for the UTS at 900°C (measured at Stork Herron), revealed any dependence of mechanical properties on the sample location in a bonded bar (Figure 16). The high-temperature testing results appeared to show a high scatter in the data (Table 5). However, a detailed analysis of the results showed that the real scatter was very low, since all the tested samples could be subdivided into two groups: those with failure occurring along the joints, and those with failure occurring far away from the joints (Figure 20). As is clear from the testing data (Table 5), the samples that failed off the joint showed much smaller ultimate tensile strength at 900°C than those that failed along the joint.

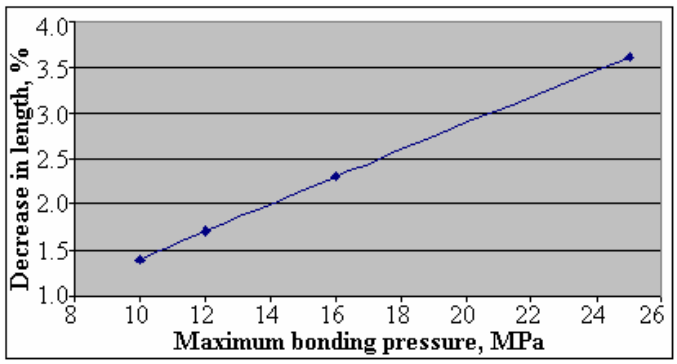

Figure 17: Dependence of Change in Length on Maximal Bonding Pressure at 1270°C

This fact explains why the data scatter in this series of experiments was so large. The UTS values of the samples that failed away from the joints represented the strength of the base alloy itself, rather than that for the joints, and those low values could not characterize joint strengths. Thus, in order to make a comparison with the UTS for MA-956, the average of the hot UTS values for the samples that failed only along the joints were used. Among the samples that failed along the joints, data scatter was fairly low. Indeed, all failed at a stress in the range from 45 MPa / 6.5ksi to 48 MPa / 7.0 ksi. The highest values were obtained under the optimum bonding pressure. It was established that the latter at 1270°C should not exceed 12 MPa / 1.7 ksi (Figure 21). Based on the data presented in Figure 22, it is possible to specify that plastic deformation during joining should not result in

a change in the sample length of more than 3%, otherwise, the macro- and microstructural changes depicted in Figures 8 and 9 dramatically decrease mechanical properties. The best UTS results (45 MPa / 6.5 ksi - 48 MPa / 7.0 ksi) for the bonded, unrecrystallized ODS superalloy (obtained without a following heat treatment) represented **41-44%** of the UTS for commercially-available MA-956 at 900°C {110 MPa / 15.9 ksi (taken from the graph – Figure 23) [12]}.

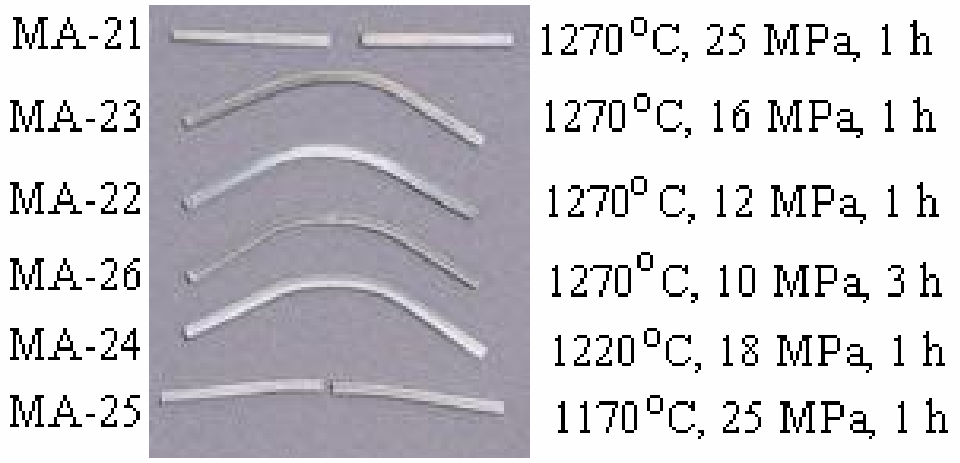

Figure 18: Unrecrystallized Samples after Flexural Test

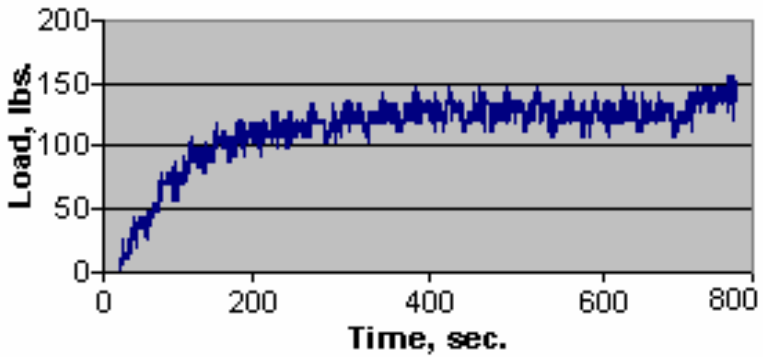

Figure 19: Flexural Testing Profile for Sample MA-24

Creep testing of sample MA-21 at 1000°C, 7 MPa / 1 ksi did not result in failure after over 265 hours. At 14 MPa (2 ksi) time to failure significantly decreased (Table 5). The samples bonded at 1170 and 1220°C failed in approximately the same time, whereas the sample bonded at 1270°C under optimum conditions survived 50% longer than those joined at lower temperatures. The creep testing results for sample MA-26 showed that an increased bonding time led to a drop in creep resistance by an order of magnitude, probably due to coarsening of oxide inclusions during a long dwell. All these samples broke along the joints (Figure 24). As well as with UTS testing, during creep testing some samples failed away from the joints. The samples bonded at 1270°C and with pressure over 16 MPa / 2.3 ksi failed in a very short time far away from the joints due to significant damage made by this excessively high pressure to the bulk material.

Table 5: Joining Parameters and Mechanical Properties of Bonded Incoloy MA-956 Superalloy

#	Bonded pieces	Bonding parameters			Change in length, %	Cold flexural		Hot (900°C) tensile			Creep (1000°C)	
		Temperature, °C	Maximal pressure, MPa / ksi	Soak time, h		Stress, MPa / ksi	Rupture	Strength MPa / ksi	Average for samples failed along joint MPa / ksi	Rupture off / along joint	Time to rupture, h	Rupture off / along joint
MA-25	A1D1A1 A1D1A2	1170	25 / 3.6	1	1.6	78 / 11.3	yes	46 / 6.7 48 / 7.0 44 / 6.4	48 / 7.0	off along off	10.0	along
MA-24	A1C1A1 A1C1A2	1220	18 / 2.6	1	2.5	91 / 13.2	no	37 / 5.4 42 / 6.1 48 / 7.0	45 / 6.5	off along along	8.0	along
MA-26	A1C1A3 A1D1A3	1270	10 / 1.4	3	1.4	76 / 11.0	no	54 / 7.8 25 / 3.6 43 / 6.2	48 / 7.0	along off along	1.5	along
MA-22	A1B1A1 A1B1A2	1270	12 / 1.7	1	2.7	80 / 11.9	no	46 / 6.7 48 / 7.0 39 / 5.6	48 / 7.0	off along off	15.3	along
MA-23	A1A1A3 A1B1A3	1270	16 / 2.3	1	5.4	80 / 11.9	no	25 / 3.6 24 / 3.5 18 / 2.6	-	off off off	3.0	off
MA-21	A1A1A1 A1A1A2	1270	25 / 3.6	1	10.4	23 / 3.3	yes	35 / 5.0 21 / 3.0 21 / 3.0	-	off off off	2.0	off
Solid MA-956 [12]		-	-	-	-	-	-	110 / 16.9	-	-	-	-

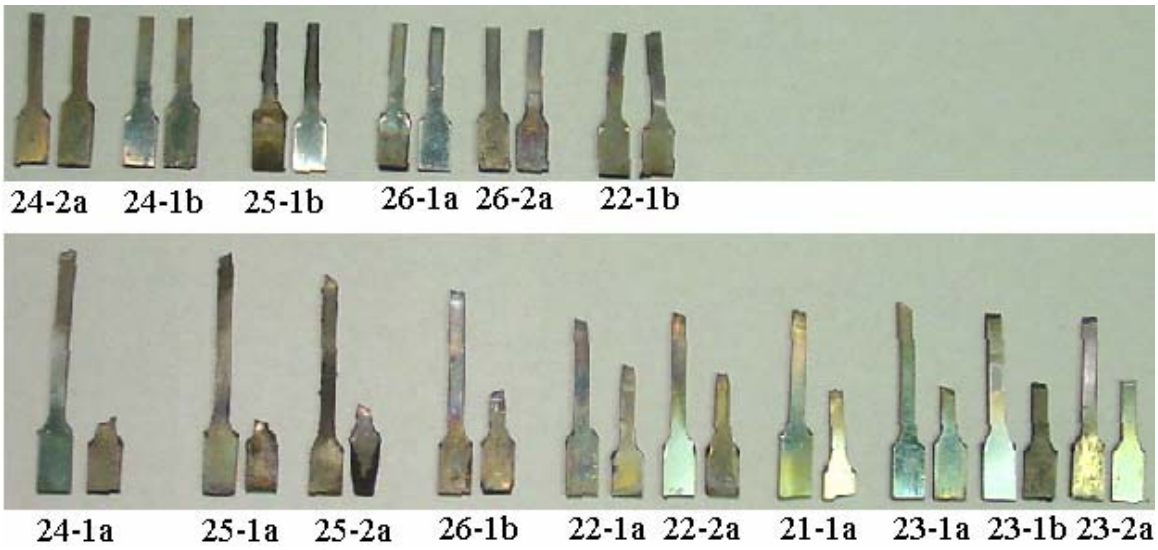

Figure 20: Unrecrystallized MA-956 Samples after Tensile Test at 900°C Failed along Joint (Upper Row) and off Joint (Lower Row)

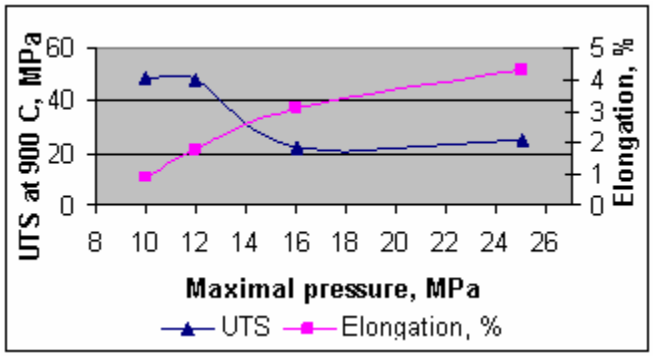

Figure 21: Dependence of Hot UTS for Samples Joined at 1270°C on Bonding Pressure

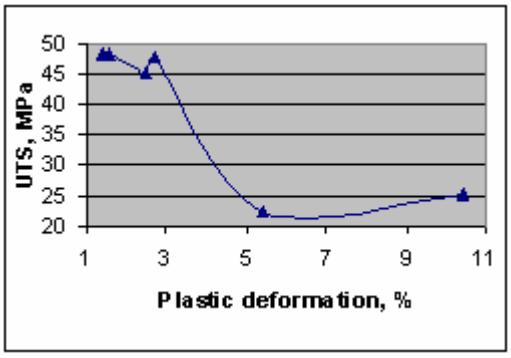

Figure 22: Dependence of Hot UTS on Plastic Deformation during Bonding

The results obtained at this stage showed that ODS superalloy may be bonded by the plasma-assisted process. Without post-joining recrystallization, the hot UTS of the bonded samples was 41-44% of that for the bulk material. These relatively low values suggested that recrystallization and grain growth across a joint only occurred partially during bonding (a conclusion which was confirmed by SEM investigation), and the high-temperature strength did not approach that of the bulk material. The next step of the current

investigation was to perform plasma-assisted bonding of unrecrystallized ODS FeCrAl, followed by a recrystallization heat treatment.

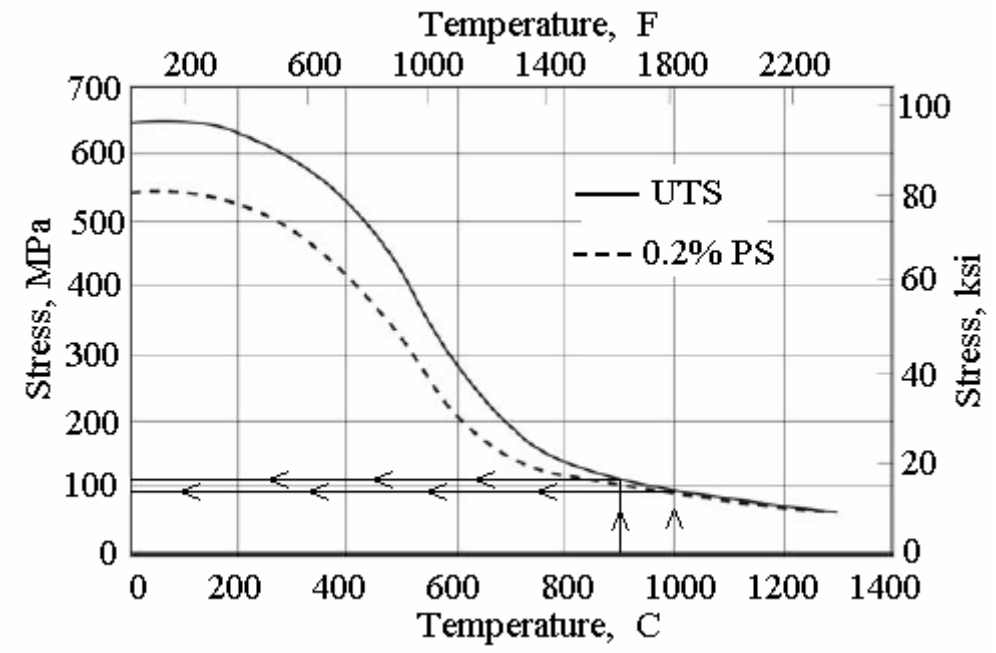

Figure 23: High Temperature Strength of MA-956 [12]

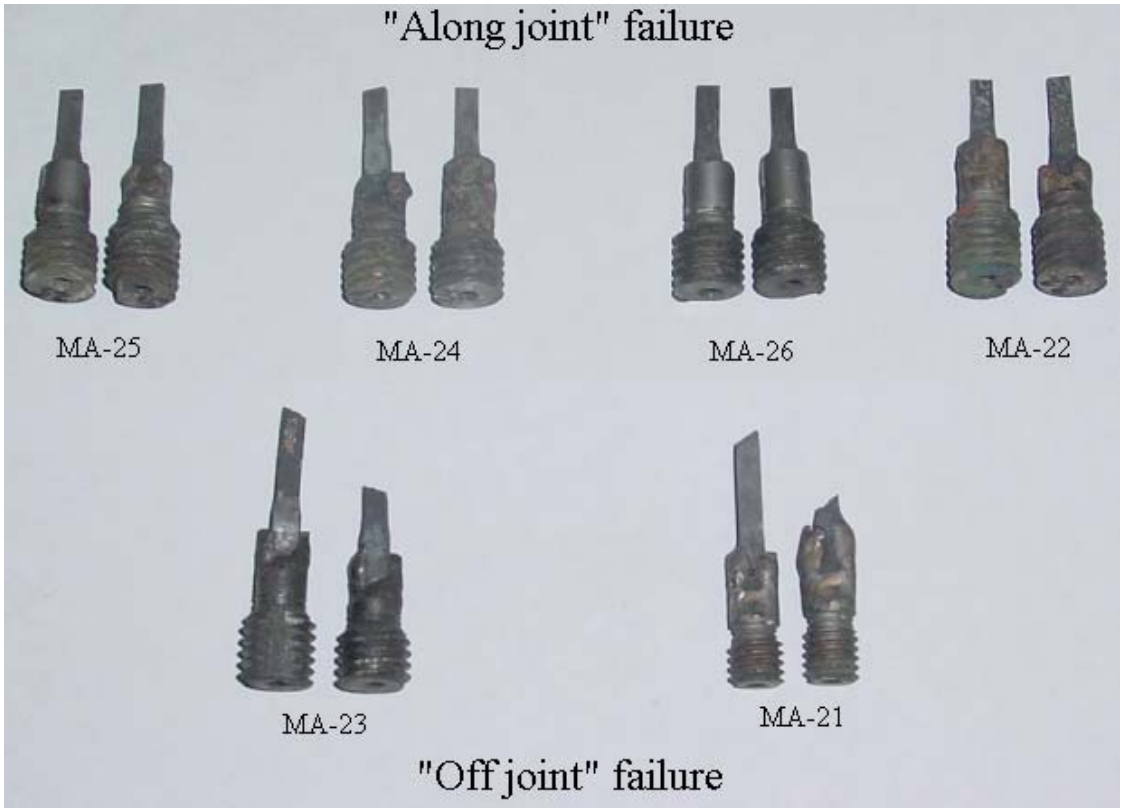

Figure 24: Creep Testing Samples Failed Along and Off Joints

3.2.2. Bonding Unrecrystallized ODS Superalloys with Post-Bonding Heat Treatment

Joining of unrecrystallized pieces was carried out in accordance with the procedure described in Section 2.3. The quality of the bonding was characterized by incrementally-loaded creep test at 1000°C at ORNL and WMT&R with different time-pressure profiles. Two sets of 20 mm (0.75") OD bonded samples (see Section 2.4) have been made. All the samples tested at ORNL were produced from PM2000 (lot KKL-4) unrecrystallized material. Unfortunately, due to the above mentioned problems with supply of ODS alloys, the samples tested at WMT&R were made from both PM2000 and MA-956.

In this series, the optimum pressure for each bonding temperature was established, as was done for the recrystallized samples. At each temperature, the first sample was bonded at a low pressure without noticeable change in the sample size. For the next sample at the same temperature, pressure was increased, and the sample dimensional change was measured. Joining was repeated until the sample became noticeably distorted (curved). It is worth noting that, at the joining temperature of 1275°C for MA-956 and 1380°C for PM2000, the samples tolerated unexpectedly high pressures. This may be explained by grain growth and an increase in compressive strength resulting from recrystallization. Some experiments were carried out a few times to correct for abnormal sample distortion or instrumental uncertainties.

The bonded rods for creep testing are presented in Figures 25 and 26. Metallographic analysis at ORNL showed that, after plasma-assisted bonding at temperature of 1220°C and higher, samples experienced full recrystallization **including grain growth across the joint** (Figure 27)**.** This did not occur in samples bonded at 1170°C. In order to provide full recrystallization in all samples, the latter, after bonding, were recrystallized at 1380°C (for PM2000) or at 1285°C (for MA-956) for 1 hour in an argon atmosphere.

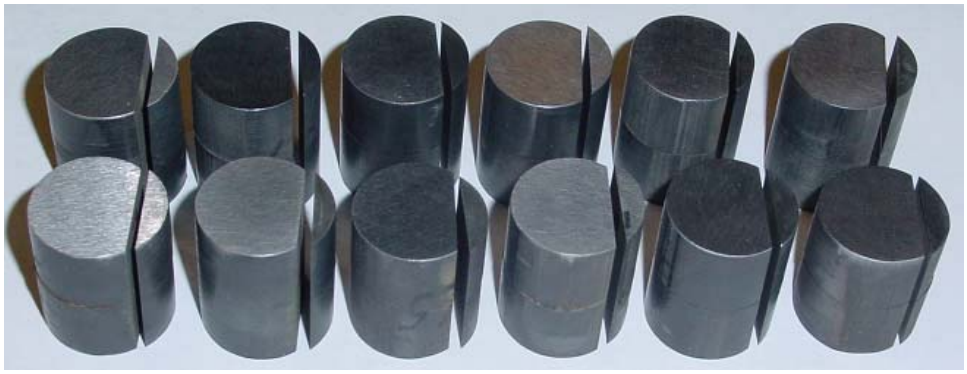

Figure 25: Bonded PM2000 Samples for High Temperature Tensile Test at ORNL

In the best samples, grains grew fully across the joints (Figures 28 a, b). However, even in such samples, the bonding lines were still visible inside grains, presumably due to very fine (100-200 nm) alumina inclusions (Figures 28 c, d) marking the junction. Subsequent TEM examination revealed that the apparent remaining bonding lines were an optical illusion due to the presence of aligned alumina inclusions from the original bonded surfaces, but that there was no change in alloy lattice structure across the bond, indicating that the inclusions had not impeded grain growth [14]. Besides those submicron inclusions, the interface may contain some

other flaws. The bulk PM2000 alloy contains a number of fairly large, rounded oxide particles. If the latter are situated at the interface in the same proportion as in the bulk material (in this case the distance between two neighboring inclusions is usually greater than 100 μm), those oxides did not appear to prevent grain growth across the joint during bonding or heat treatment. If the distance between adjacent oxide particles was smaller than ≈20 μm, grain growth across the bonding line did not occur (compare Figures 28 e and f).

Figure 26: Bonded MA-956 and PM2000 Samples for Creep Testing at WMT&R

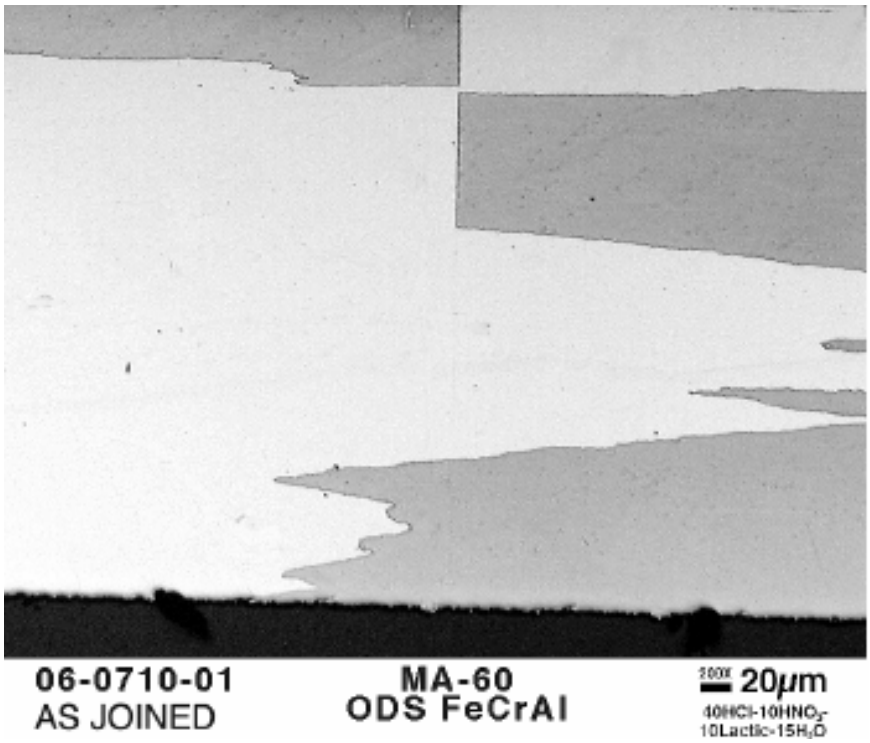

Figure 27: Grain Growth Across Joint during Plasma-Assisted Bonding

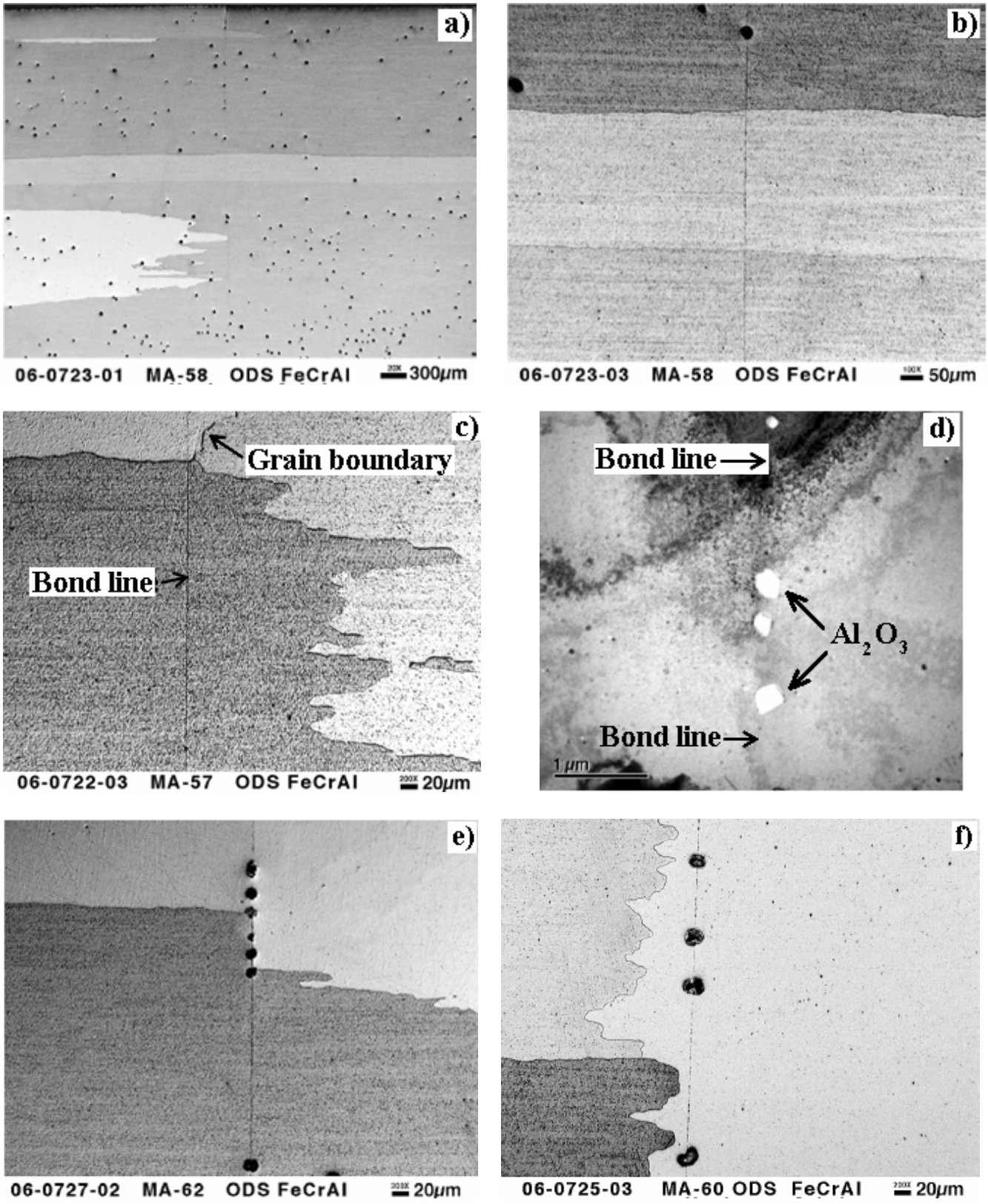

Figure 28: Microstructure of Bonded PM2000 after Recrystallization

High concentrations of oxide inclusions (Figure 29 a) at the interface not only prevents grain growth across the bonding line, but also weakens the interface, thus possibly decreasing the joint mechanical properties. The most serious flaws, which were found in only some of the bonded samples, were cracks (Figure 29 b) located immediately along the joint, or in the vicinity of the latter. Such cracks were presumably generated by fast heating and cooling. Fast heating for bonding was used in order to preclude recrystallization from occurring before the joining temperature could be reached (since the initial goal was to ensure recrystallization simultaneously with bonding, thus providing grain growth across the joint). After the soak time was over, the power of the pulse-sintering machine was shut off, and the sample was cooled very quickly, since (in contrast to a regular furnace) no hot heating element surrounds the sample. It is believed that in both cases (during heating and cooling) thermal cracks may be avoided.

The 'creep' test that the ORNL used for discriminating among the different joints involved incremental loading in 3 MPa steps of specimens exposed in air at 1000°C. Testing started at 25 MPa. If, after each load increment, there was no measurable creep in a 24 hr period, the load was incremented by 3 MPa. This procedure was repeated until creep was observed, at which point the test was continued at the same loading until the specimen failed. This provided a 'threshold load' that was a useful discriminating parameter of nominal creep behavior, as well as the basis for choosing a reasonable loading value for use in conventional creep testing to determine creep rate. The testing results are presented in Table 6. The testing performed at WMT&R at 1000^{o}C followed a slightly different procedure. Since no creep occurred at low stress, the starting load was set to 40 MPa. Then the load was incremented every 6 hours by 3 MPa, no matter what strain was observed, until a sample failed (Table 7). The testing diagrams are given in Appendix.

The failures in the ORNL tests apparently did not initiate along the joint, as shown in Figure 30. The gauge width of the specimen shown was essentially two grains wide; cracking initiated in one grain, causing the other to fail by overloading [14]. The observed mode of failure: by crack-initiated transgranular brittle fracture, followed by ductile overload failure, was typical for ODS alloys [15, 16].

Table 6: High-Temperature 'Creep' Testing Results from ORNL

Sample ID	Bonded material	Bonding temperature, ^{o}C	Bonding pressure, MPa / ksi	Change in length, %	Failure stress, MPa / ksi
MA-55	PM2000	1170	7.5 / 1.1	0.8	0
MA-56	PM2000	1170	10.0 / 1.4	1.7	53 / 7.7
MA-57	PM2000	1170	12.5 / 1.8	2.4	77 / 11.1
MA-58	PM2000	1170	15.0 / 2.2	5.0	
MA-59	PM2000	1220	5.0 / 0.7	0.0	64 / 9.3
MA-60	PM2000	1220	7.5 / 1.1	0.3	57 / 8.3
MA-61	PM2000	1220	10.0 / 1.4	3.0	0
MA-62	PM2000	1220	12.5 / 1.8	5.6	76 / 11.0
MA-63	PM2000	1275	5.0 / 0.7	0.6	31 / 4.5
MA-64	PM2000	1275	7.5 / 1.1	1.1	45 / 6.5
MA-65	PM2000	1380	5.0 / 0.7	0.2	36 / 5.2
MA-66	PM2000	1380	7.5 / 1.1	0.2	47 / 6.8

Table 7: High Temperature Testing Results from WMT&R

Sample ID	Bonded material	Bonding			Testing			
		Temperature, °C	Pressure, MPa / ksi	Change in length, %	Duration, h	Creep, %	Failure stress, MPa / ksi	Notes
MA-53	PM2000	1170	7.5 / 1.1	0.6	24.5	0.62	49 / 7.1	
MA-49	MA-956	1170	10.0 / 1.4	1.0	44	1.25	46 / 6.7	
MA-48	MA-956	1170	12.5 / 1.8	1.9	1.9	0.15	40 / 5.8	continuous creep
MA-54	PM2000	1220	5.0 / 0.7	0.5	64	0.39	70 / 10.1	
MA-50	MA-956	1220	7.5 / 1.1	1.4	61	0.39	70 / 10.1	continuous creep
MA-43	MA-956	1220	12.5 / 1.8	3.3	102	1.25	88 / 12.8	
MA-46	MA-956	1285	5.0 / 0.7	0.7	36	1.45	55 / 8.0	continuous creep

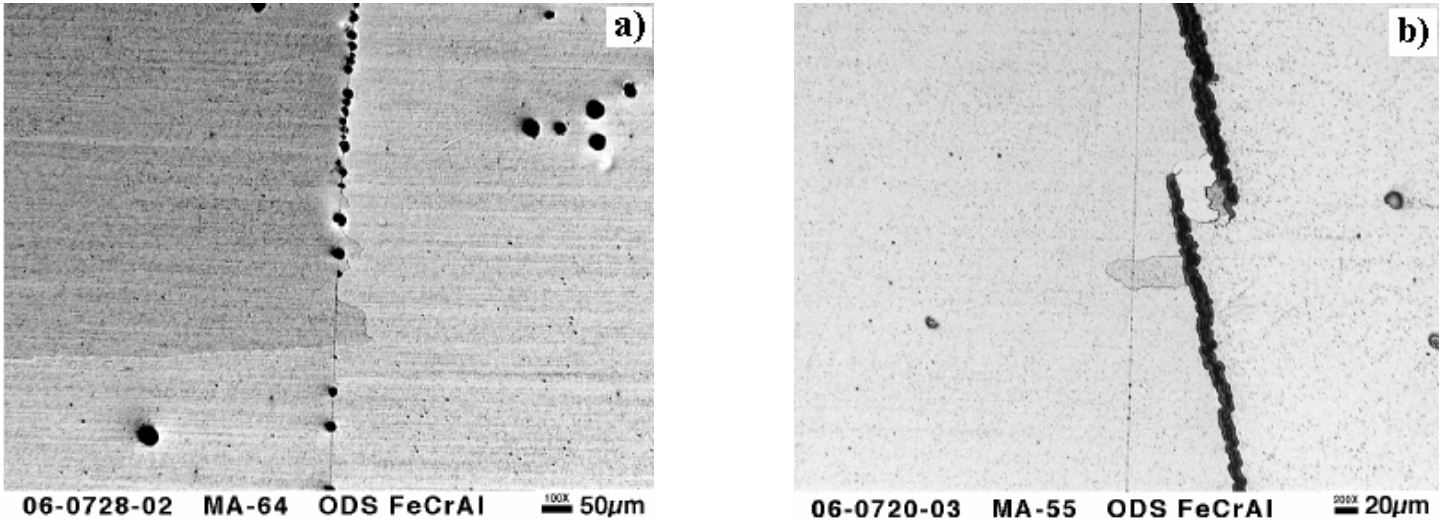

Figure 29: Flaws in Some Bonded Samples

Due to flaws of the type shown in Figure 29 two samples failed during loading. All the samples tested at the ORNL were made of PM2000, while the samples tested at WMT&R were predominantly made of MA-956. As seen in Tables 6 and 7, there was no significant difference between the best results for both alloys (although the best result was obtained with MA-956). The latter required a bonding temperature of 1220°C for the high strength joint, while PM2000 may also be successfully bonded at 1170°C if a higher pressure of (12.5 MPa) is used. Both materials, when bonded at high temperatures (close to their recrystallization temperature), demonstrated mediocre high-temperature strength.

For high creep-strength ferritic steels joined by conventional welding methods, weld factors (WFs) of 50-80% are considered to be usual, and the typical WF for weldable high-temperature Ni-base alloys is approximately 80%. Samples bonded under optimum conditions repeatedly demonstrated (in step-loading test at 1000°C) creep-rupture strengths of 70 MPa / 10.1 ksi to 77 MPa / 11.1 ksi, which make up from 78 to 86% of the solid MA-956 UTS at 1000°C while one result was **88 MPa / 12.8 ksi**, which amounts to **98% of the solid MA-956 UTS at 1000°C**.

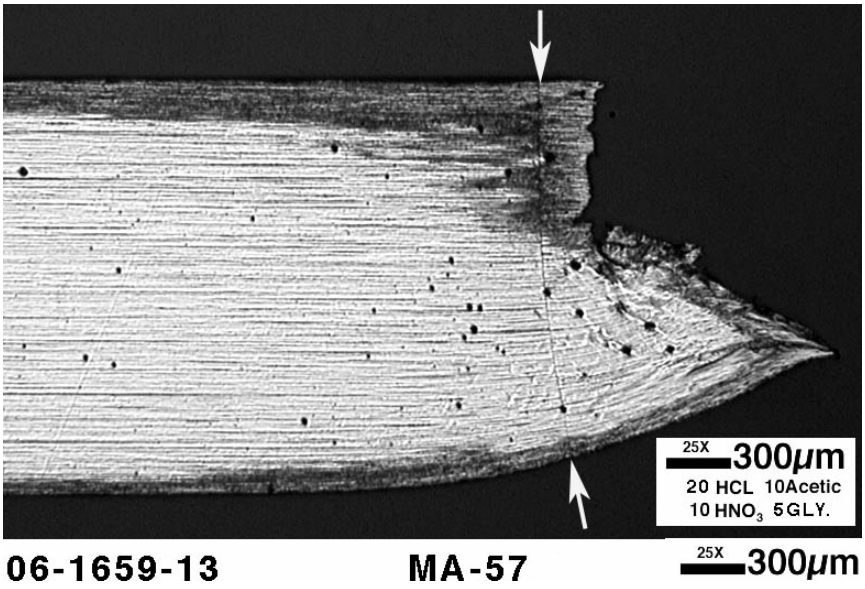

Figure 30: Macro-Section of Gauge after Failure (Bond Line is Indicated by Arrows) [14]

4. Plasma-Assisted Bonding ODS Superalloys: Tube Joint

High-temperature gas-to-gas heat exchangers represent a key application where ODS ferritic alloys can make a large impact. Those devices contain creep-resistant tubes that must be bonded in order to form heat exchanger structures. Plasma-assisted bonding, which was successfully used to produce butt joints, compulsorily involves axial pressure in order to provide a proper contact between the surfaces to be bonded, and to reliably ensure high electric current through the surfaces to be bonded. Such an axial pressure cannot be applied to long tubes of relatively small diameters.

In the course of the current project, another plasma-assisted process has been proposed which does not involve any necessity to apply axial pressure, in order to bond long tubes. Tube joining was carried out by first joining the tubes by common threading with an outer bonding ring, followed by sealing with the ODS alloy applied by the plasma-assisted process. Figure 31 illustrates the bonding scheme, and simultaneously represents an assembly for high-temperature testing. Two tubing halves (1) are joined with the threaded bonding ring (2). The length of the threaded portion of the tubes was greater by 1.5 times than the tubing diameter, in order for the thread tensile strength to be equal to that for the solid tube.

Since bonded heat exchanger tubes should be proof against gas leaks (a protection which is not provided with a simple threaded joint), the latter was sealed with a layer of FeCrAl material ('3' in (Figure 31), which had a similar chemical composition as MA-956 or PM2000, hence the same coefficient of thermal expansion. Thus, the threaded joint provides strength and integrity, while plasma-assisted layer seal the joint. Grips (4) made of creep-resistant MAR-M superalloy, connected the sample with the testing machine. The sealing was also applied between the tubes being tested and the grips, in order to equalize the diameter of this joint with that for the tube-bonding ring joint, in order to avoid premature failure near the grips, since strength of the tube-bonding ring joint was the primary interest. The assembly, fully prepared for high-temperature testing, is shown in Figure 32.

The step-loading test at 1000^{o}C in air was carried out at Stork-Herron Testing Lab (Cleveland, OH). The test started at 25 MPa / 3.6 ksi. While it was intended that pressure was incremented every 24 hours by 3 MPa / 0.4 ksi, in practice the uploads were made at arbitrary times. The testing results are presented in Figure 33. The sample failed at **49 MPa / 7.1 ksi after 377 hours.** The sample after testing is illustrated in Figure 34. As seen, failure occurred at the tube-grip joint, while the tube-bonding ring joint remained intact. This gives a reason to believe that the strength of the proposed joint was greater than 49 MPa / 7.1 ksi.

Unfortunately, only hoop creep data for PM2000 at 1000^{o}C were found in the literature, which could not be compared with the results of the current testing. However, tube axial creep data for MA-956 at 1000^{o}C are available. If it is assumed that the properties of PM2000 and MA-956 are similar, the literature data for MA-956 tubes can be compared with the results for the PM2000 tube joint in the current tests. Figure 35 contains the literature data for MA-956 tube creep resistance. The latter is dependent on tube diameter and grain size, and varies at 1000^{o}C from ≈ 44 MPa / 6.4 ksi to 74 MPa / 10.7 ksi (the numbers are taken from the plot). Thus, **the MER-bonded tube creep resistance value falls in the range for that for solid ODS ferritic superalloy tubes**. It was mentioned earlier that weld factors (WFs) of 50-80% are considered to be usual, and the typical WF for weldable high-temperature Ni-base alloys is approximately 80%. In light of this statement, the MER result for a tube joint seems to be fairly high. However, it is unknown whether the proposed approach (Figure 31) provides a fully-sealed joint, which has to be a subject for further investigations.

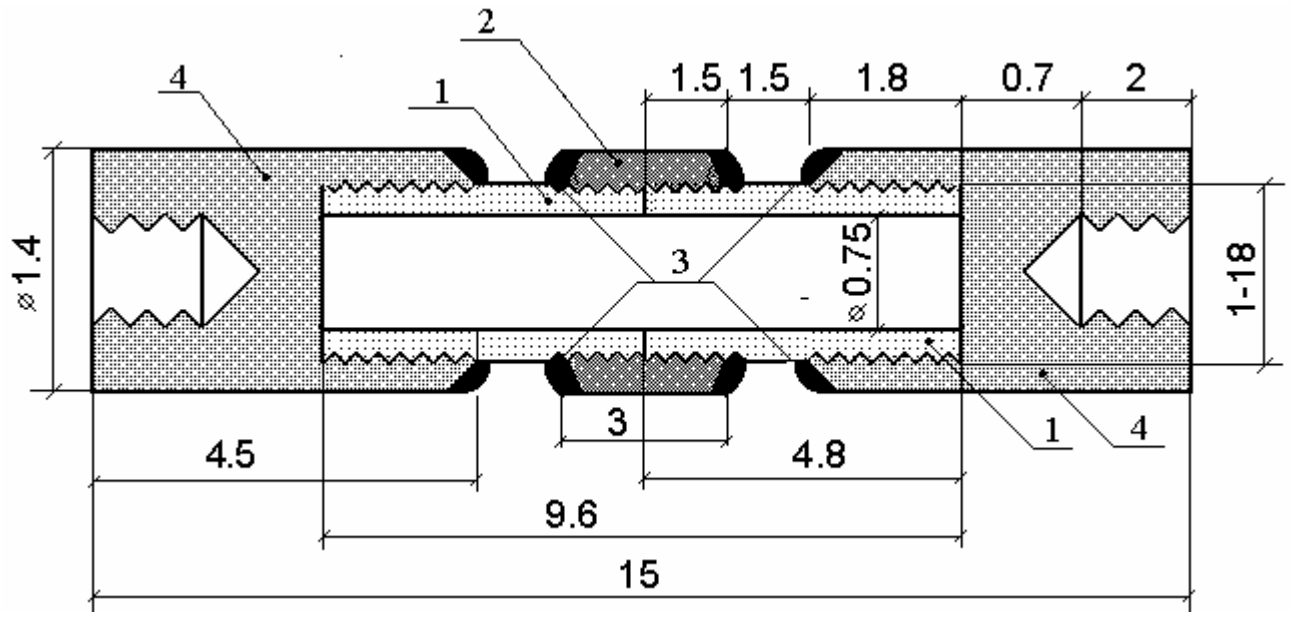

Figure 31: Bonded Tube Testing Sample Scheme

1 – Tubes to be bonded
2 – Bonding ring
3 – Plasma-assisted sealing
4 – Pulling grips

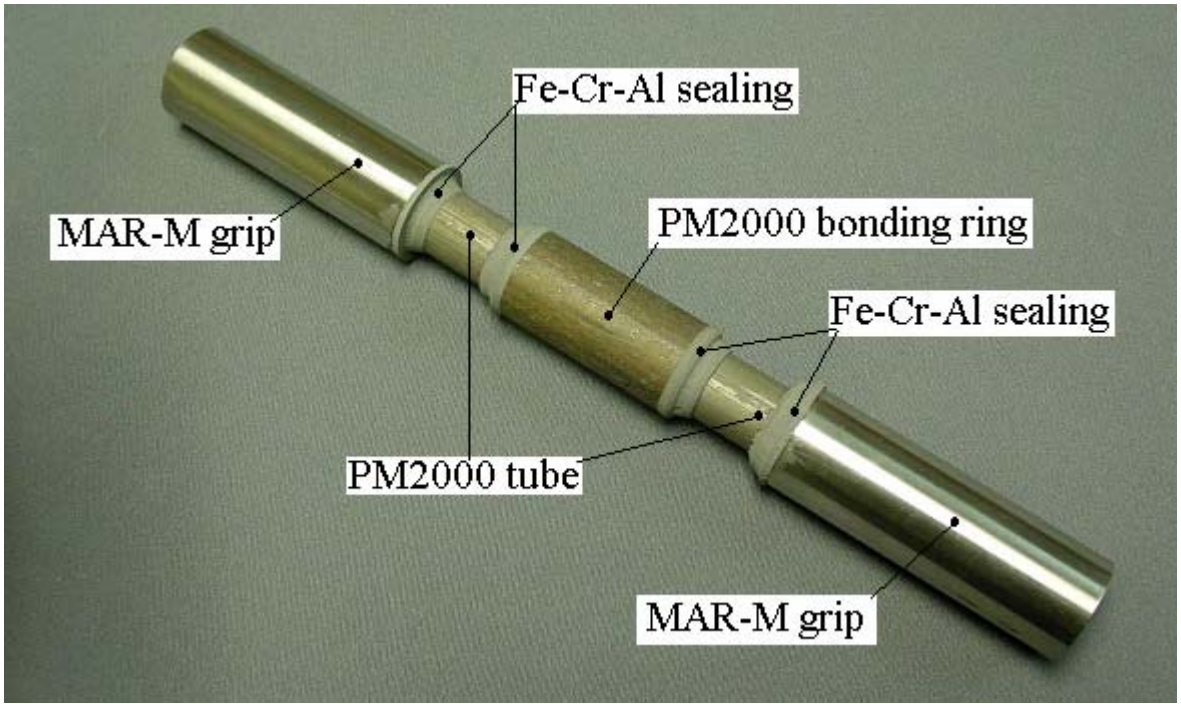

Figure 32: Tube Sample Assembly for High Temperature Testing

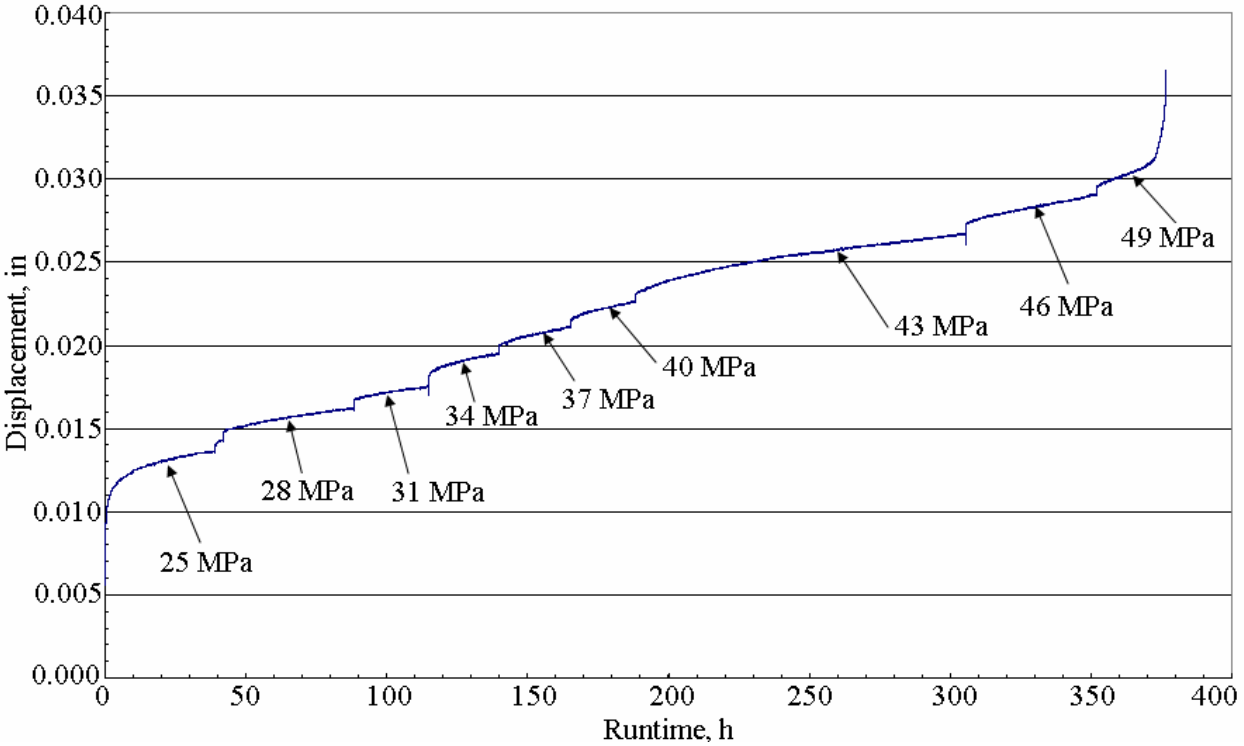

Figure 33: MER Tube Sample High Temperature (1000°C) Testing Results

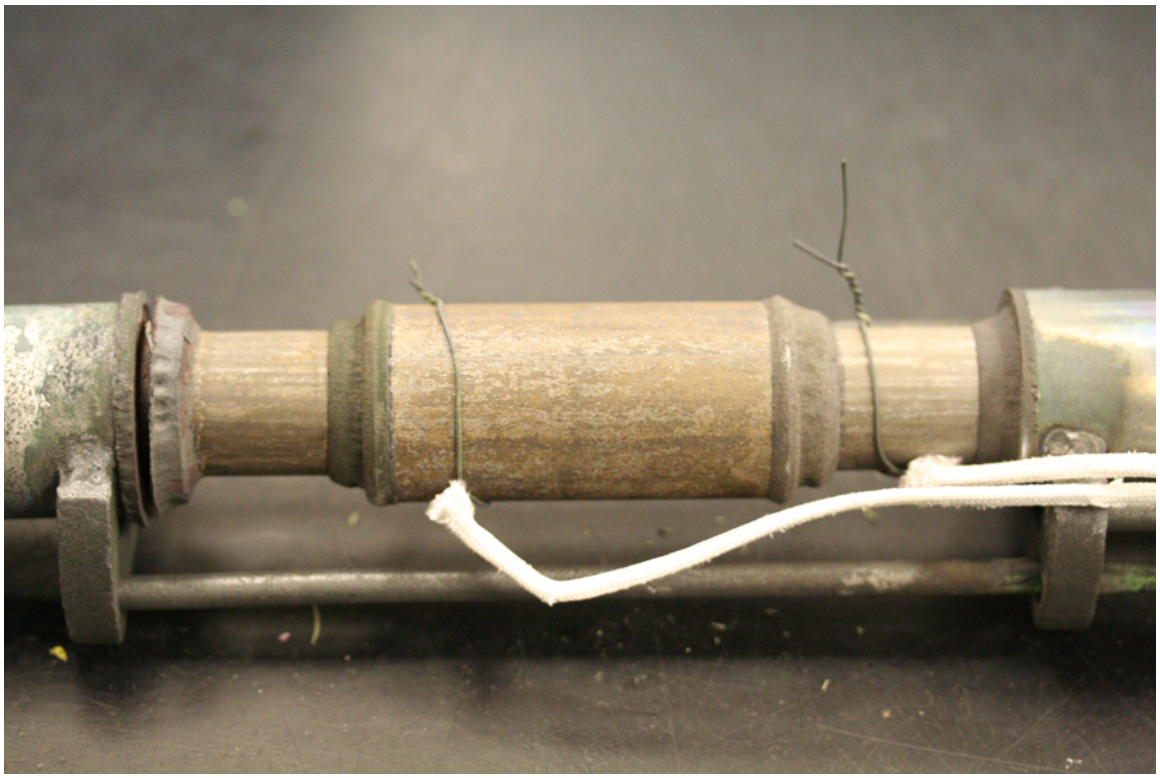

Figure 34: Bonded PM2000 Tube Sample Failed at 49 MPa far off Joint

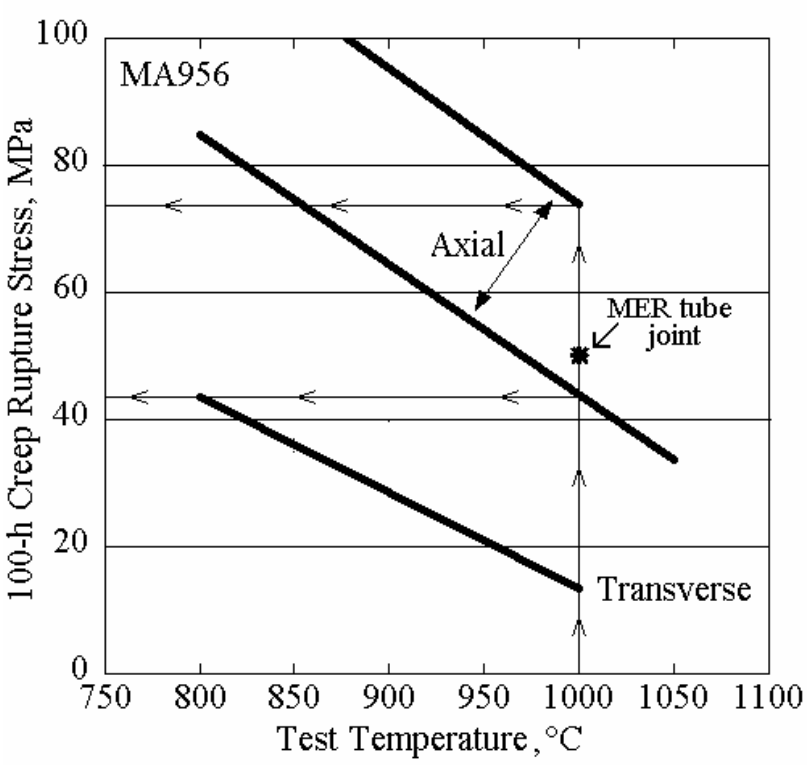

Figure 35: ODS Ferritic Superalloy Tube Creep Properties [17]

5. Conclusions

1) Plasma-assisted butt bonding of recrystallized ODS ferritic superalloy does not provide grain growth across a joint, and thus does not result in strong bonding.

2) Plasma-assisted butt bonding of unrecrystallized ODS ferritic superalloy without a following heat treatment results in partial secondary recrystallization and partial grain growth across a bonding line. The ultimate tensile strength at 900°C of such a joint is 45-48 MPa / 6.5-7.0 ksi, which is 41-44% of that for monolithic, commercially-available MA-956 alloy at 900°C.

3) Plasma-assisted butt bonding of unrecrystallized ODS ferritic superalloy, followed by heat treatment, results in full, secondary y recrystallization and grain growth across the bonding line. An incrementally-loaded creep test at 1000°C of these joints resulted in rupture values from 70 MPa / 10.1 ksi to 77 MPa / 11.1 ksi, which are 78-86% of the monolithic MA-956 UTS at 1000°C. The best result was **88 MPa / 12.8 ksi**, which amounts to **98% of the solid MA-956 UTS at 1000°C.**

4) The best results were obtained at 1220°C, 12.5 MPa / 1.8 ksi pressure, 1 hour soak time, 63 Hz frequency and 70% duty cycle. Bonding at the recrystallization temperature does not lead to a high-strength joint. At each bonding temperature, there is a pressure threshold above which irreversible microstructural changes in the bulk material occur, resulting in poor high-temperature mechanical properties. During plasma-assisted

bonding, thermal cracks may appear along the joint or in its vicinity. Heating and cooling rates should be adjusted to avoid thermal crack formation.

5) Tube bonding of a commercially-available recrystallized ODS ferritic superalloy with plasma-assisted sealing resulted in failure at **49 MPa / 7.1 ksi in 377 hours** during step-loading testing at 1000°C, which **falls in the same range as for solid ODS ferritic superalloy tubes**.

REFERENCES

1 Hedrich H.D., Mayer H.D., Haufler G., Kopf M., and Reheis N. Joining of ODS Superalloys. Proc. Conf. on Materials for Advanced Power Engineering, Coutsouradis D. et al., Eds., Kluwer Academic Publishers, Dordrecht, 1994, p. 789-798.

2 Kad B.K., Heatherington J. H.McKamey C., Wright I., Sikka V. and Judkins. Optimization of High-Temperature Hoop Creep Response in ODS-Fe_3Al Tubes. www.osti.gov/energycitations/purl.cover.jsp?purl=/835677-Vqvohm/native/

3 Klueh R. L., Shingledecker J. P., Swindeman R. W. and Hoelzer D. T. Oxide dispersion-strengthened steels: a comparison of experimental and commercial steels. Journal of Nuclear Materials**,** 2005, **341**, N2-3, p. 103-114.

4 Wright I.G., Bornstein N.S., Dyadko E.G., and Dryepondt S.N. Enabling the Practical Application of Oxide Dispersion-Strengthened Ferritic Steels. In Proc. 20th Ann. Conf. on Fossil Energy Materials, Editor R.R. Judkins, 2006, p. 30-38.

5 Zhang G., Chandel R.S., Seow H.P., and Hng H.H. Microstructural Features of Solid-State Diffusion Bonded Incoloy MA-956. Materials and Manufacturing Processes, 2003, **18**, N4, p. 599-608.

6 Kang C.Y., North T.H., and Perovic D.D. Microstructural Features of Friction Welded MA-956 Superalloy Material. Metals and Materials Transactions A, 1996, **27A**, N12, p. 4019-4029.

7 Verpoort C. Method of Manufacturing a Workpiece of Any Given Cross-Sectional Dimensions from an Oxide Dispersions Hardened Nickel Based Superalloy with Directional Coarse Columnar Crystals. US Patent 4817858, B23K 20/02, B21K 3/04, 04.04.1989.

8 Jahnke B. Metallic Joining Material. US Patent 4678635 C/22C 19/05, 07/07/1987.

9 Groza J.R., Risbud S.H., and Yamazaki K. Plasma Activated Sintering – a Novel Versatile Consolidation Process. Proceeding of a Symposium on Plasma Synthesis and Processing of Materials, TSM Annual Meeting, February 22-25 1993, Denver, CO.

10 Groza J.R. and Zavaliangos A. Sintering Activation by External Electric Field. Material Science and Engineering A: Structural Materials, 2000, **287**, N2 p. 171-177.

11 Nishimoto K., Saida K., and Tsuduki R. Effect of Pulse-Electric Current on Densification Behaviour of Bonded Interlayer of Oxide-Dispersion-Strengthened Superalloys Joint. J. Japan Inst. Metals, 2001, **65**, N8, p. 747-755.

12 www.specialmetals.com/products/incoloyalloyma956.htm

13 www.plansee.com/hlw/ods_superalloys_pm_2000_ENG_HTML.htm

14 Tatlock G.J., Dyadko E.G., Dryepondt S.N., and Wright I.G., Pulsed Plasma-Assisted Diffusion Bonding of ODS-FeCrAl Alloys. Submitted to Met. Trans. 2006.

15 Weigert W.H., Henricks R.J., Tensile and Creep-Rupture Behavior of Two Advanced, Oxide Dispersion-Strengthened Sheet Alloys. In Superalloys 1980, Eds. J.K. Tien et al., ASM 1980, p. 575-584.
16 Whittenberger J.D. Tensile and Creep Properties of Experimental Oxide Dispersion-Strengthened Iron-Base Sheet Alloy MA956E at 1365K, Met. Trans. A, 1978, **9A**, p. 101-110.
17 Wright I.G., Pint B.A., and Lu Z.P. Overview of ODS Alloy Development. Presented at the 19th Ann. Conf. on Fossil Energy Materials, Marriott Hotel, Knoxville, Tennessee, 2005, May 9-11.

Appendix: WMT&R Testing Profiles

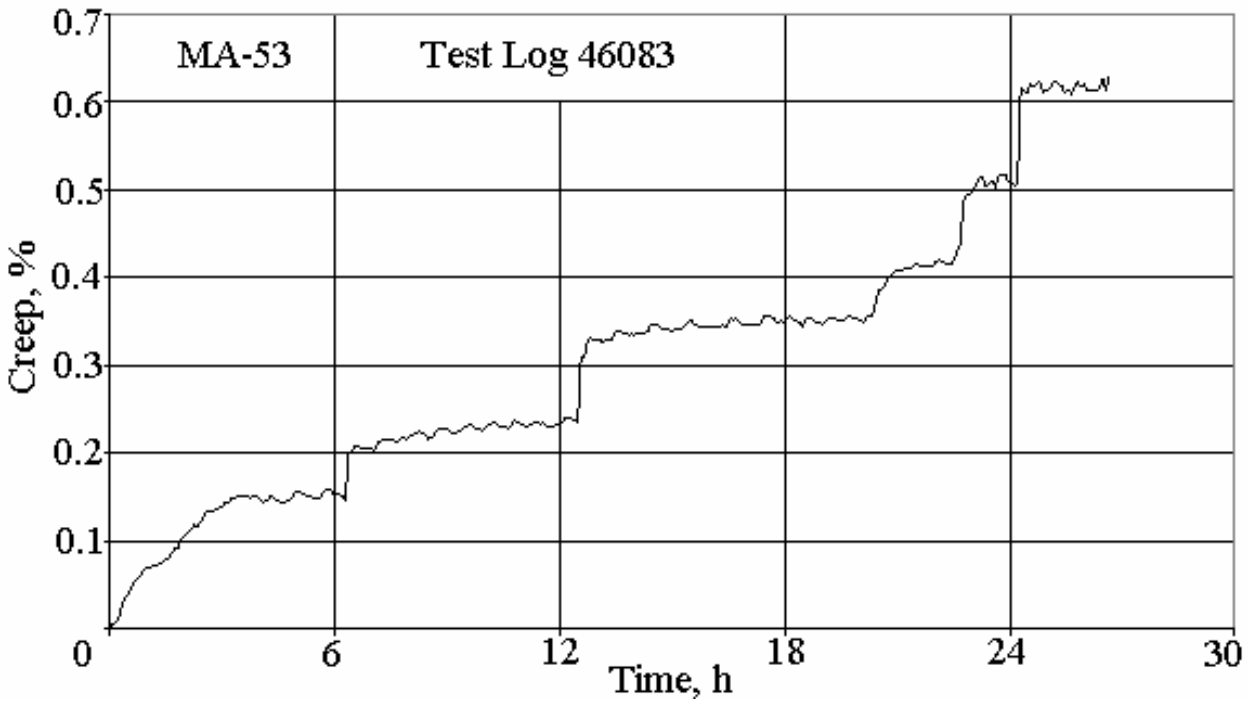

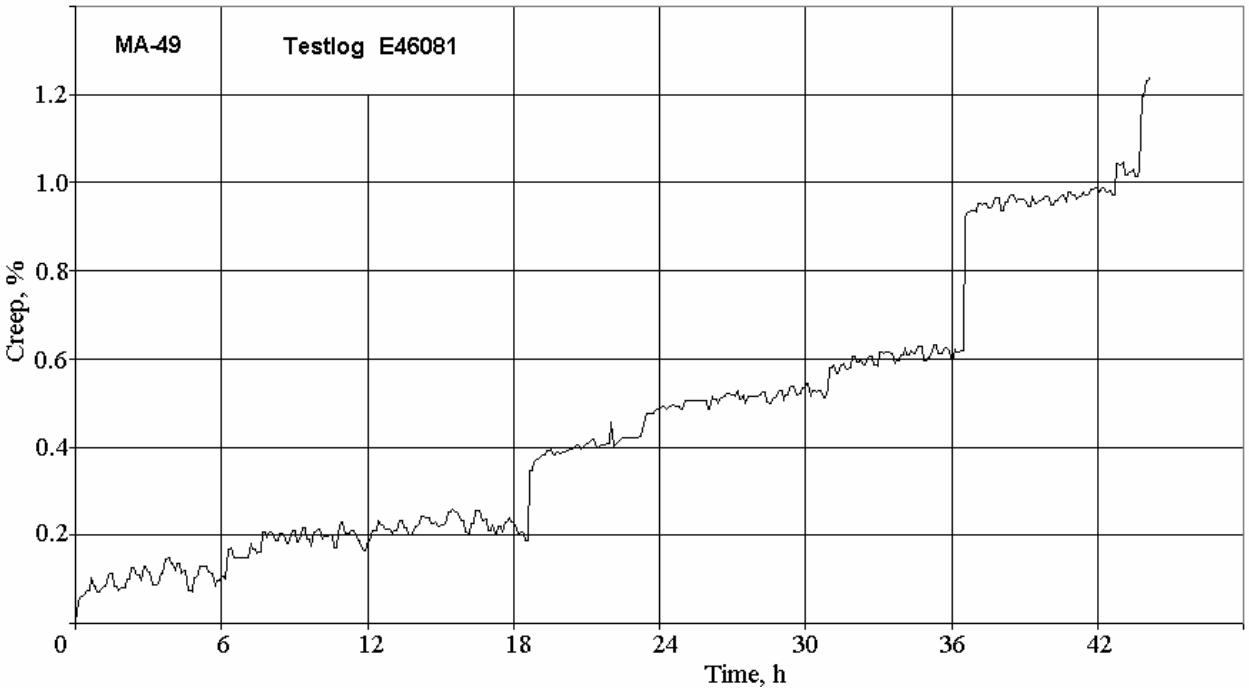

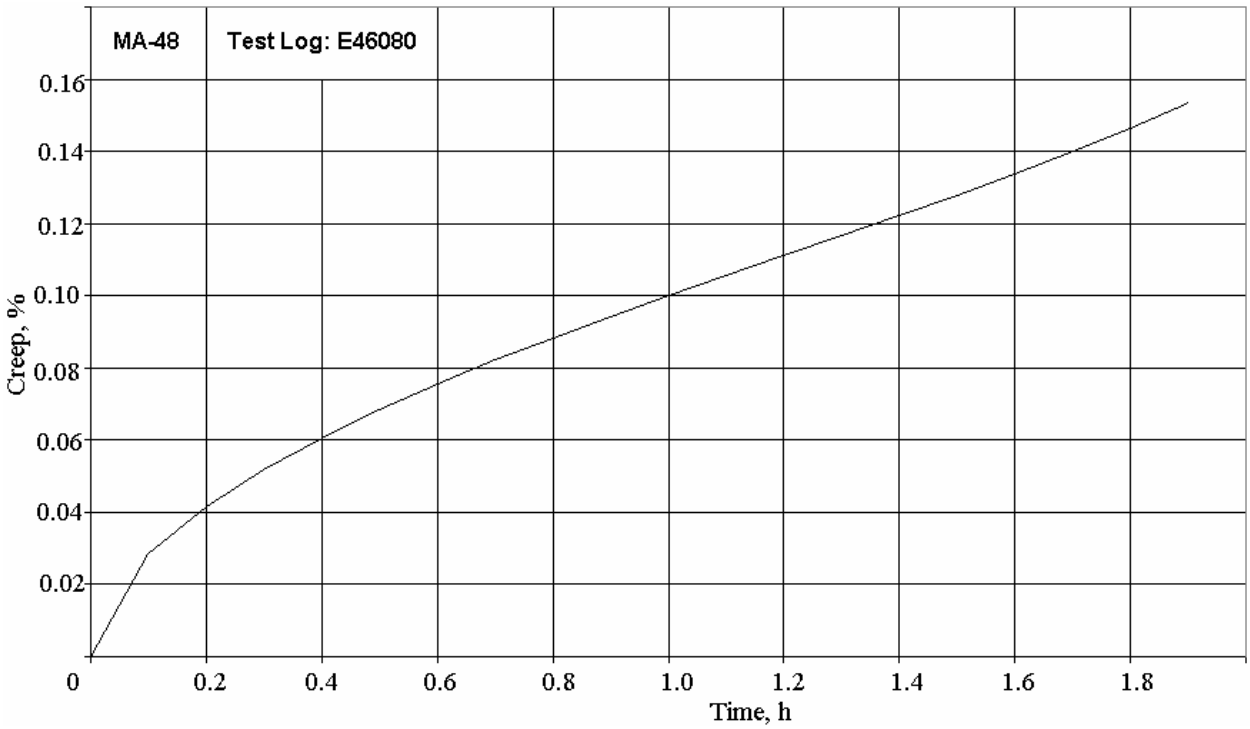
MA-48
Test Log: E46080
Creep, %
0.16
0.14
0.12
0.10
0.08
0.06
0.04
0.02
0
0.2
0.4
0.6
0.8
1.0
1.2
1.4
1.6
1.8
Time, h

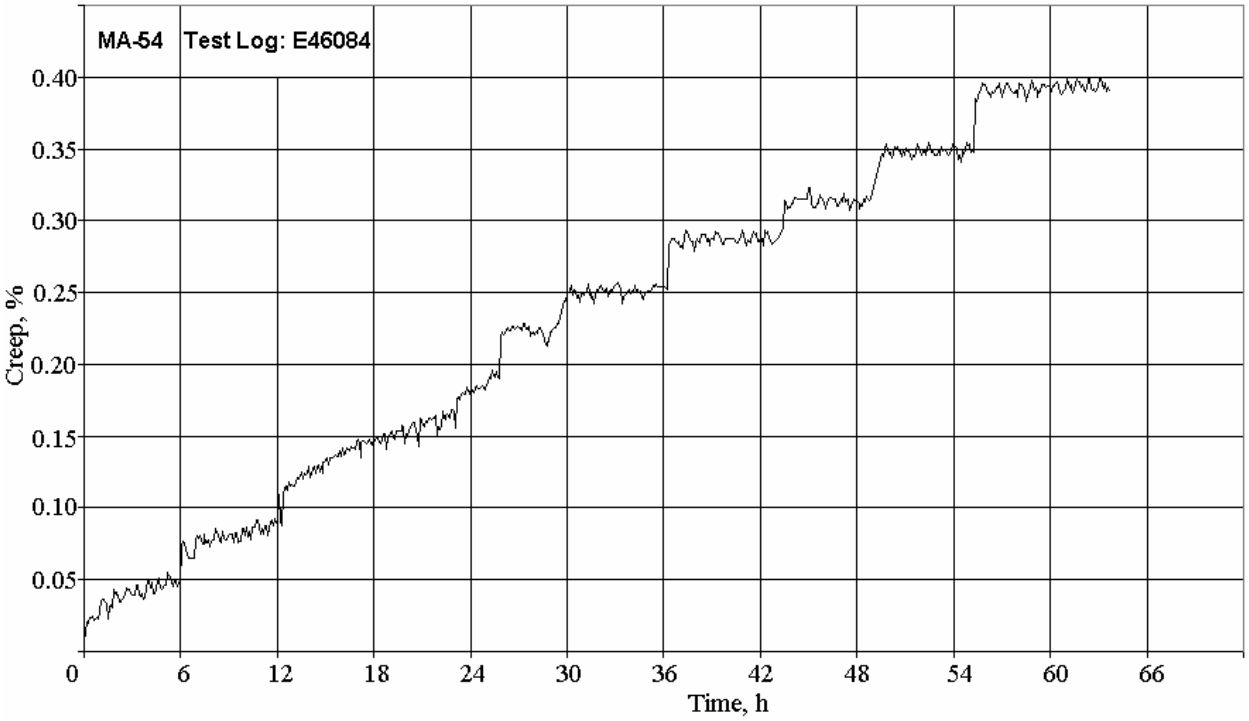
MA-54
Test Log: E46084
Creep, %
0.40
0.35
0.30
0.25
0.20
0.15
0.10
0.05
0
6
12
18
24
30
36
42
48
54
60
66
Time, h

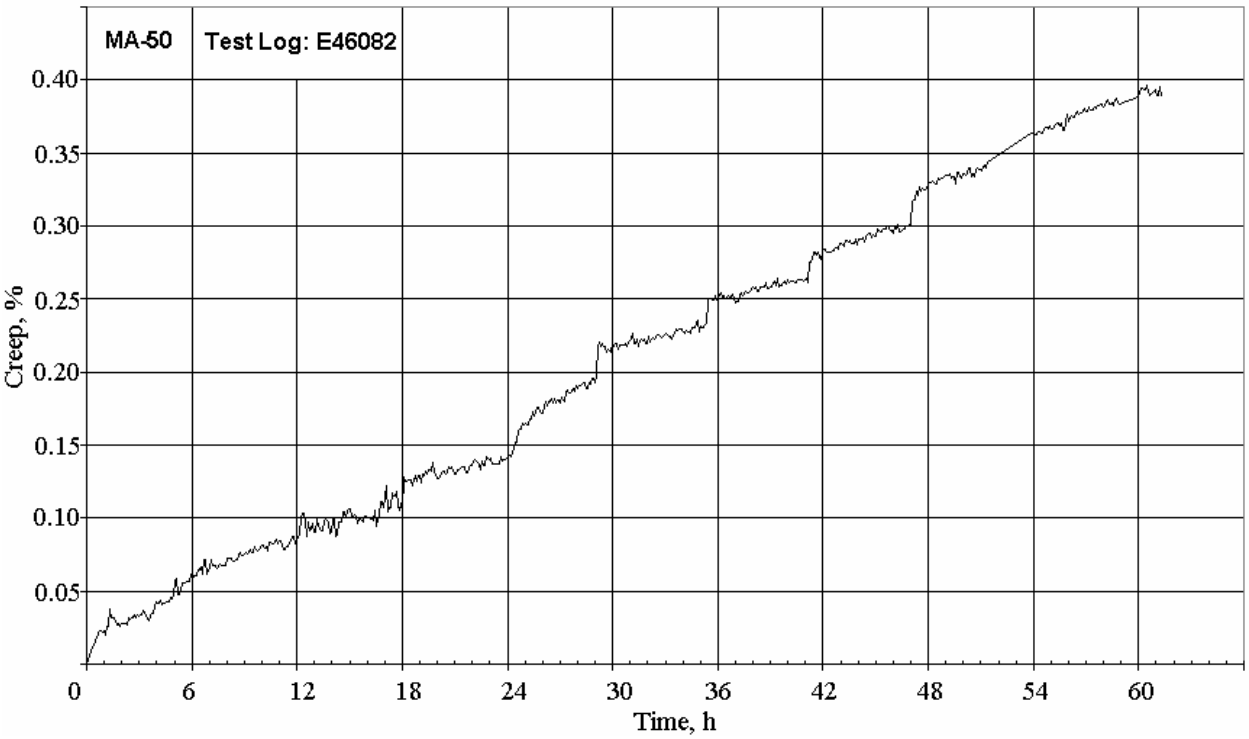
MA-50
Test Log: E46082
Creep, %
0.40
0.35
0.30
0.25
0.20
0.15
0.10
0.05
0
6
12
18
24
30
36
42
48
54
60
Time, h

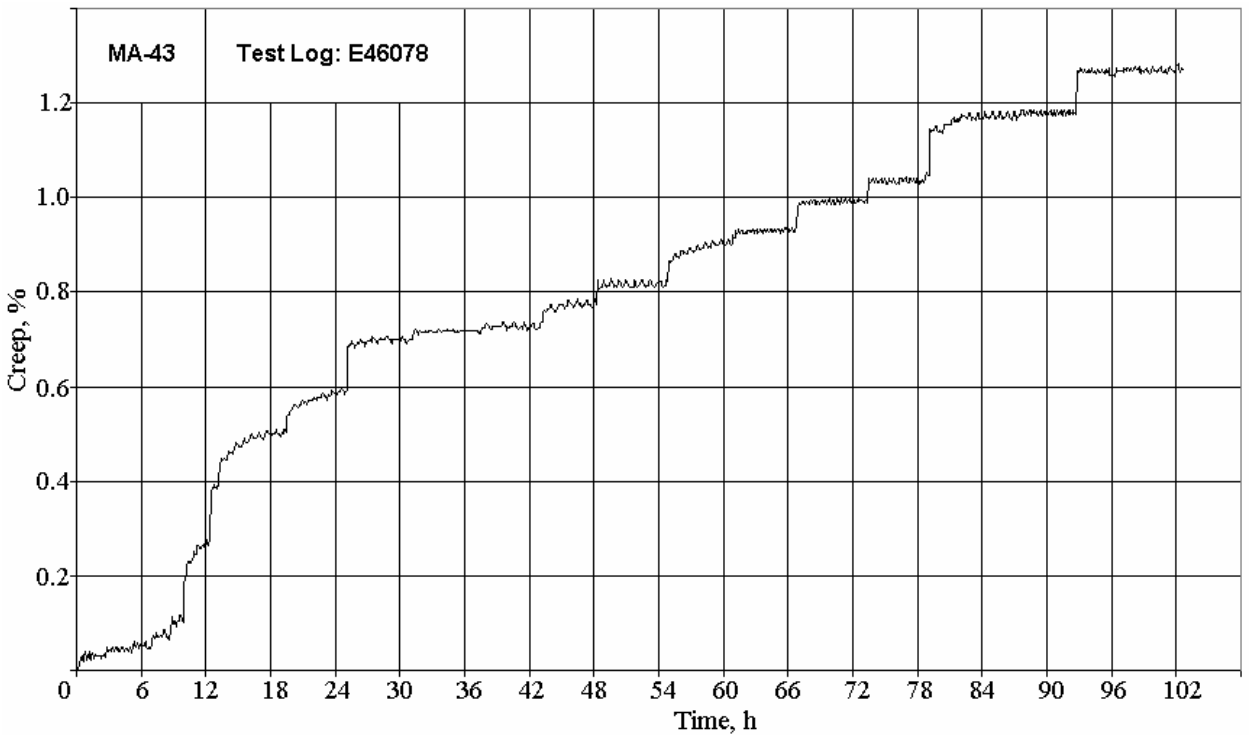
MA-43
Test Log: E46078
Creep, %
1.2
1.0
0.8
0.6
0.4
0.2
0
6
12
18
24
30
36
42
48
54
60
66
72
78
84
90
96
102
Time, h

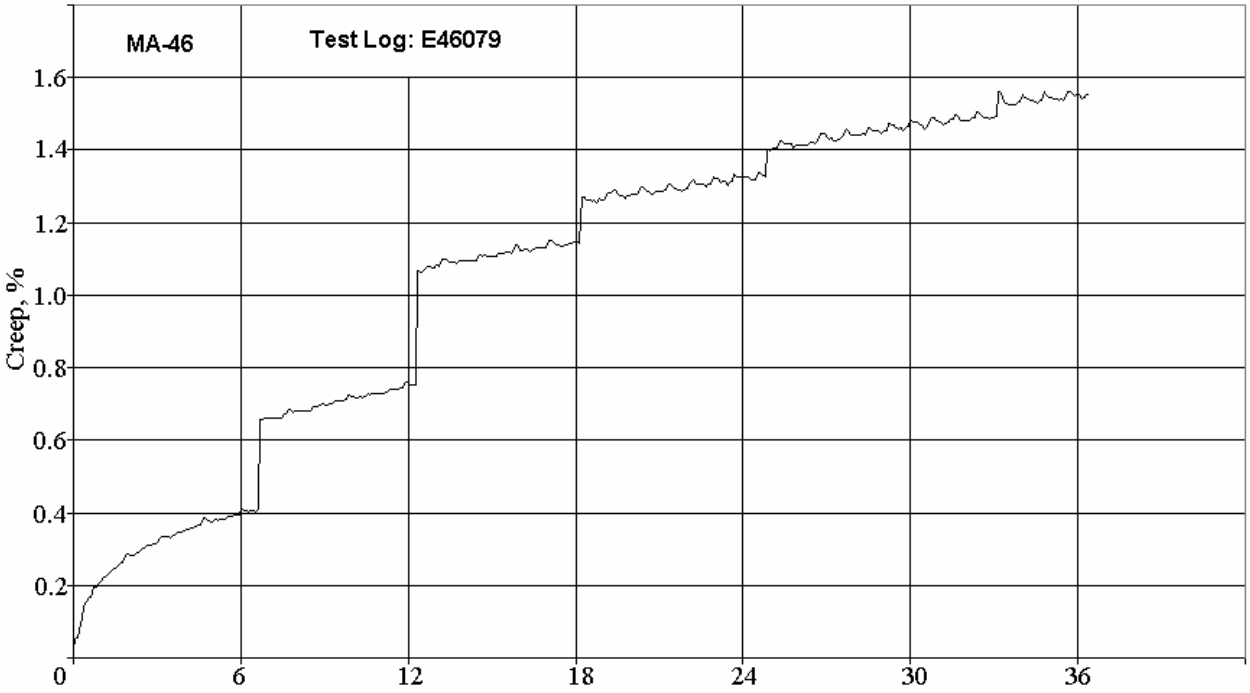
MA-46
Test Log: E46079
Creep, %
1.6
1.4
1.2
1.0
0.8
0.6
0.4
0.2
0
6
12
18
24
30
36